CHAPTER 4

RESULTS

4.1 Appropriate basis set for the Li-C_{60} complexes

The results of SCF calculations for different basis sets with and without BSSE were displayed in Table 4.1. The calculation was given up after 150 hours for the DZP basis set.

Table 4.1 Optimal stabilization energies with and without BSSE (ΔE_{BSSE} and ΔE_{SCF} in kcal.mol^{-1}) and corresponding distances from center of the C_{60} to Li (r_{BSSE} and r_{SCF} in Å) and time requires (CPU time in hour for Li-C_{60} complexes on the IBM RISC 6000/530H Workstation) calculated from the STO-3G, 6-31G and DZP basis sets.

Basis sets	ΔE_{SCF}	ΔE_{BSSE}	BSSE	r_{SCF}	r_{BSSE}	r_{shift}	CPU time (hrs)
STO-3G	3.4478	3.4478	0	5.24	5.24	0	1.5
6-31G	-2.3533	-2.3533	0	8.00	8.00	0	13.5
DZP	-	-	-	-	-	-	>150

4.2 Intermolecular potential function

4.2.1 Li@C_{60} endohedral potential function

The resulted SCF energies, calculated using the 6-31G basis set, for the endohedral Li@C_{60} complexes are shown in Table 4.2. They are also plotted (Fig. 4.1) as a function of the distance from center of C_{60} to Li for different

angles, defined by the vectors parallel to z-axis and to each trajectory, C5, B65, C6 and B66. Note that corresponding angles for the trajectories C5, B65, C6 and B66 are 31.7°, 48.5°, 69.1° and 90°, respectively (see Fig. 3.2).

The endohedral stabilization energies are well represented by equation (4.1). The obtained fitting parameters are A=9.4508x10^{-8} kcal.mol^{-1}, B=10.3541 Å^{-1} and C=20.4486 kcal.mol^{-1}. In addition, the standard deviation of the fit is 5.10 kcal.mol^{-1}.

The distribution plot for all data points obtained from the SCF calculations (ΔE_{SCF}) and from the fit (ΔE_{FIT}) is shown in Fig. 4.2(a). The ΔE_{SCF} and ΔE_{FIT} as a function of the distance from center of C_{60} to Li for the trajectory C6 are compared in Fig. 4.2(b).

$$\Delta E(r) = A\exp(Br) + C \qquad (4.1)$$

Table 4.2 Stabilization energies and corresponding distances for the endohedral $Li@C_{60}$ complexes in different trajectories.

r (Å)	ΔE (kcal.mol^{-1})			
	B66	C6	C5	B65
1.00	18.917701	20.603642	18.568396	19.421476
1.10	18.156832	20.000640	17.437503	20.002121
1.20	17.444720	19.737969	16.845783	19.349941
1.30	17.398385	19.888355	17.607026	21.220687
1.40	17.099532	20.723144	21.053635	24.065678
1.50	17.163522	22.366177	23.739724	26.208761
1.55	17.653466	23.537469	25.150300	28.973896
1.60	18.512362	25.217838	26.637250	31.108746
1.65	19.885612	26.939987	28.990236	33.763893
1.68	21.064258	28.325400	29.585885	35.796114
1.72	22.525913	29.326777	31.813001	36.386466
1.75	24.851761	32.183126	33.536040	40.432454
1.80	28.837980	35.565740	37.05125	42.958692
1.90	60.267177	43.091034	45.23256	53.020707
2.00	72.265542	54.217418	82.639980	71.163545

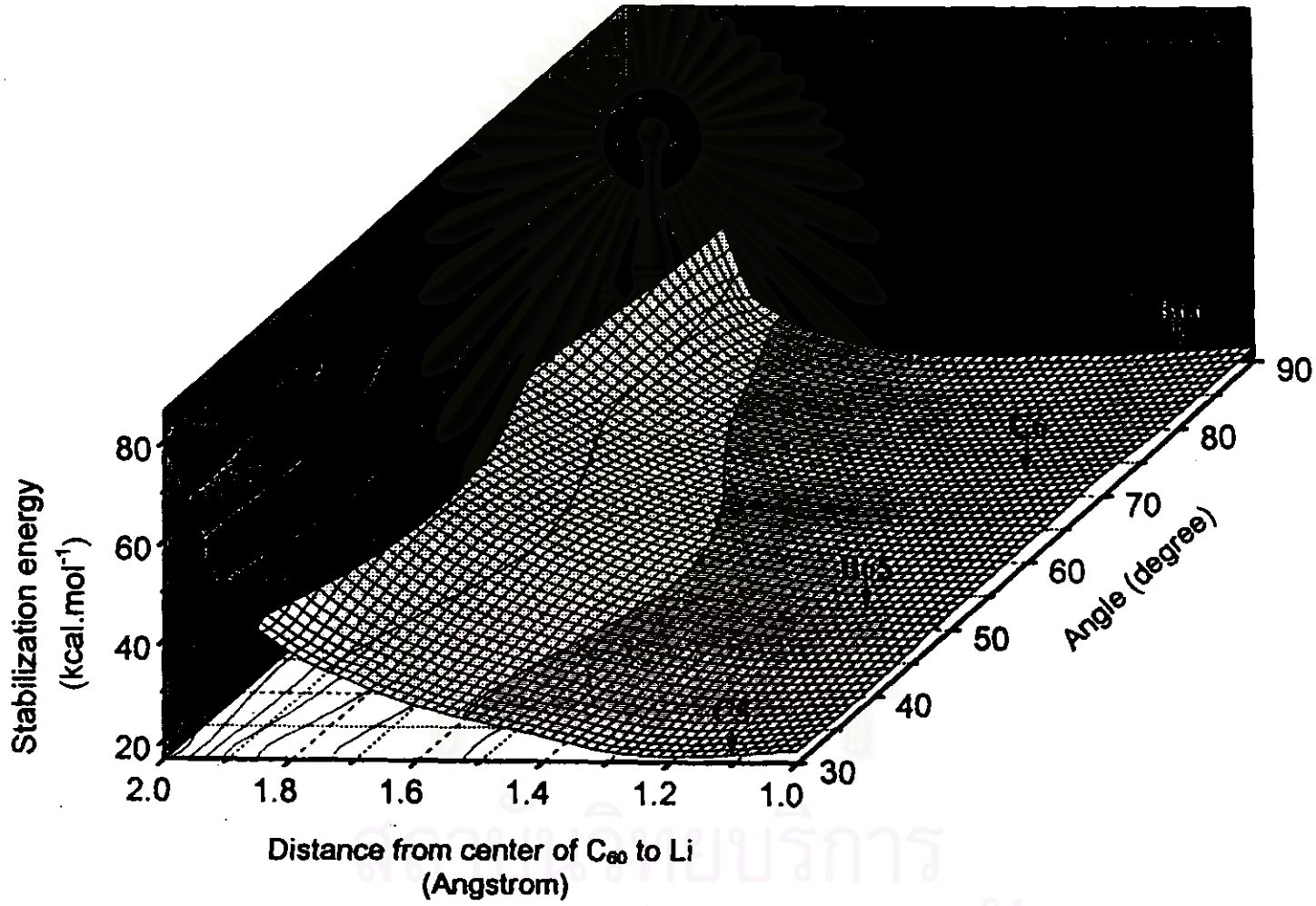

Figure 4.1 The potential energy surface for the endohedral $Li@C_{60}$ complexes as a function of the distance from center of C_{60} to Li (see text for more detail).

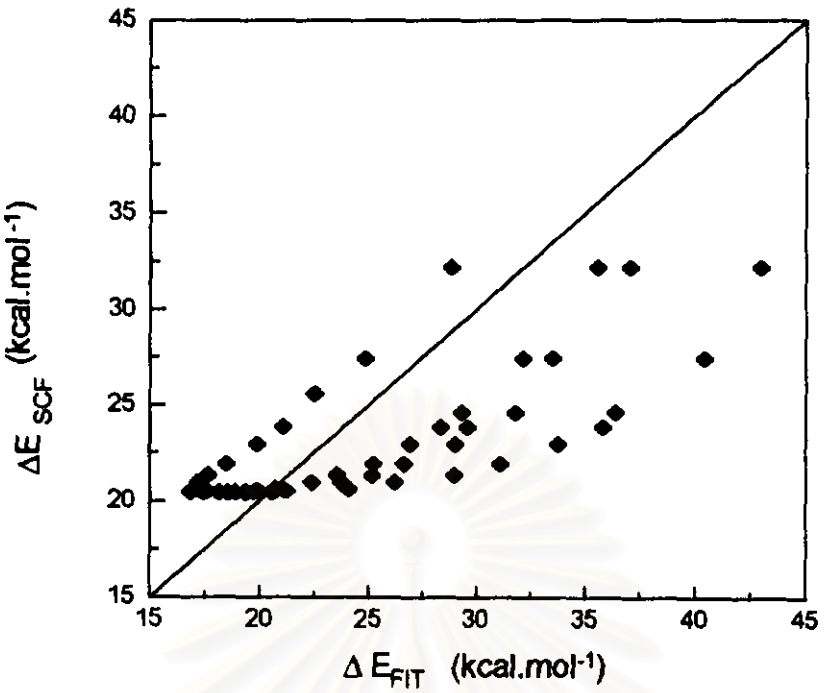

(a)

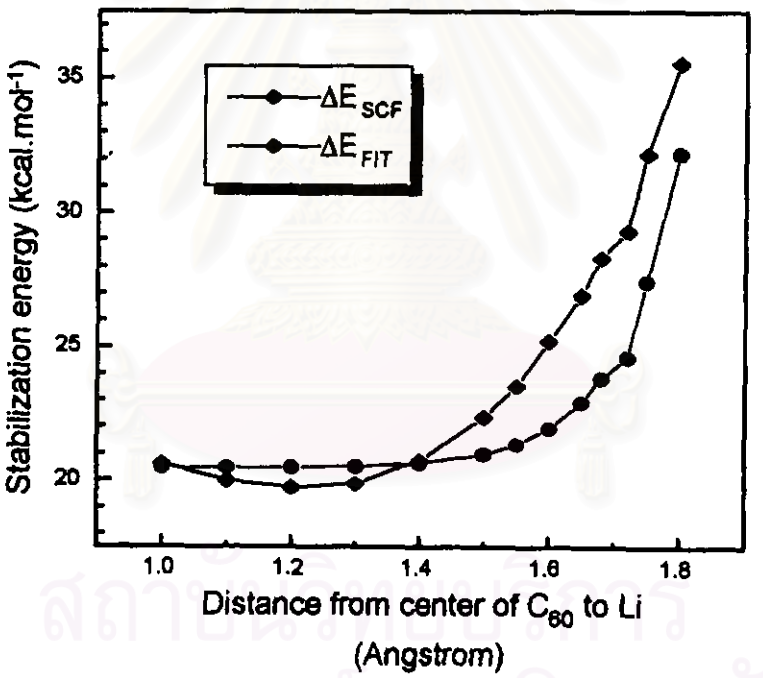

(b)

Figure 4.2 (a) Comparison of the stabilization energies for the endohedral Li@C_{60} complex obtained from the SCF calculation (ΔE_{SCF}) with those from the fit (ΔE_{FIT}).

(b) ΔE_{SCF} and ΔE_{FIT} versus distance from center of C_{60} to Li for trajectory C6.

4.2.2 LiC_{60} exohedral potential function

The stabilization energies and potential energy surface for the exohedral LiC_{60} complexes are shown in Table 4.3 and Fig. 4.3, respectively. The optimum functional form is

$$\Delta E(r) = A\exp(-Br) + C \quad (4.2)$$

where A=2.6903x10^5 kcal.mol^{-1}, B=1.8378 Å^{-1} and C=2.0442 kcal.mol^{-1}. Furthermore, the standard deviation is 2.07 kcal.mol^{-1}. The ΔE_{SCF} and ΔE_{FIT} are compared in Fig. 4.4(a). The potential energy curve for trajectory C6 is displayed in Fig. 4.4(b).

Table 4.3 Stabilization energies and corresponding distances for the exohedral LiC_{60} complexes in different trajectories.

r (Å)	ΔE (kcal.mol^{-1})			
	B66	C6	C5	B65
3.90	1205.90321	157.741458	292.127065	1162.99974
4.00	1044.21343	143.062238	238.952251	962.748633
4.10	824.677336	125.172872	189.409915	774.132405
4.50	241.398899	51.919262	54.709366	225.407281
5.00	25.746739	21.842754	27.828044	34.623455
5.20	9.414370	14.254416	18.235064	29.914469
5.40	7.451725	9.203022	10.991058	14.894767
5.60	6.224068	6.249103	7.302839	8.146588
5.80	4.900976	4.334908	5.293540	4.536172
6.00	2.888508	2.758678	3.441756	2.388127
6.20	1.844938	1.543838	2.177400	1.283194
6.40	0.343111	0.551980	1.118211	0.353753
6.60	-0.296017	-0.187309	0.089161	-0.290162
6.80	-0.833050	-0.883457	-0.513966	-0.651966
7.00	-1.311933	-1.105674	-0.791849	-0.965616
7.20	-1.521317	-1.475980	-1.235384	-1.114747
7.40	-1.716796	-1.813889	-1.355933	-1.467264
7.60	-1.959570	-2.074170	-1.894686	-1.952441
7.80	-2.159460	-2.244367	-2.131919	-2.159943
8.00	-2.277699	-2.353282	-2.269849	-2.283065
9.00	-2.011012	-1.983189	-1.992200	-2.002233
10.00	-1.876451	-1.851947	-1.848835	-1.857958

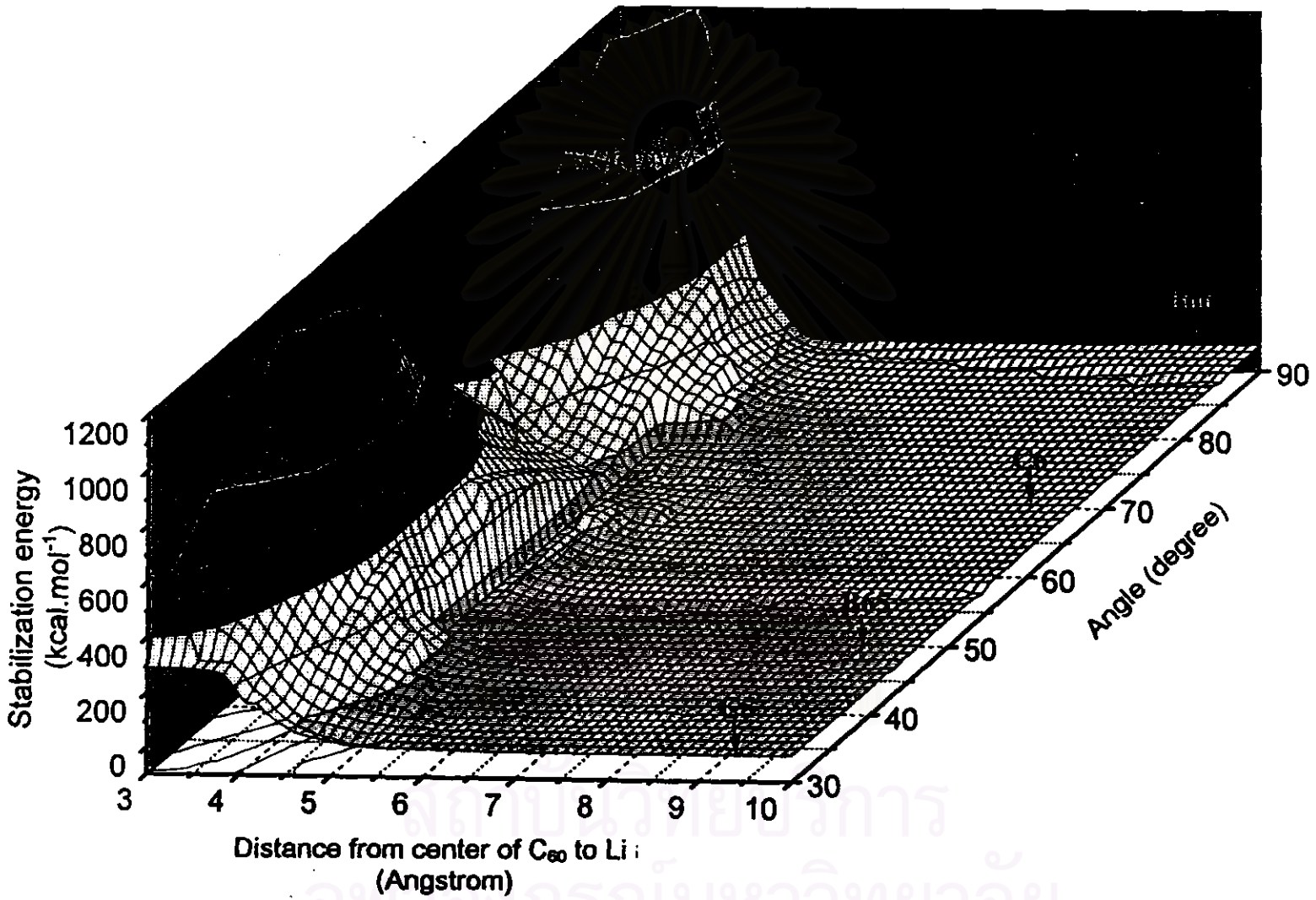

Figure 4.3 The potential energy surface for the exohedral LiC_{60} complexes as a function of the distance from center of C_{60} to Li (see text for more detail).

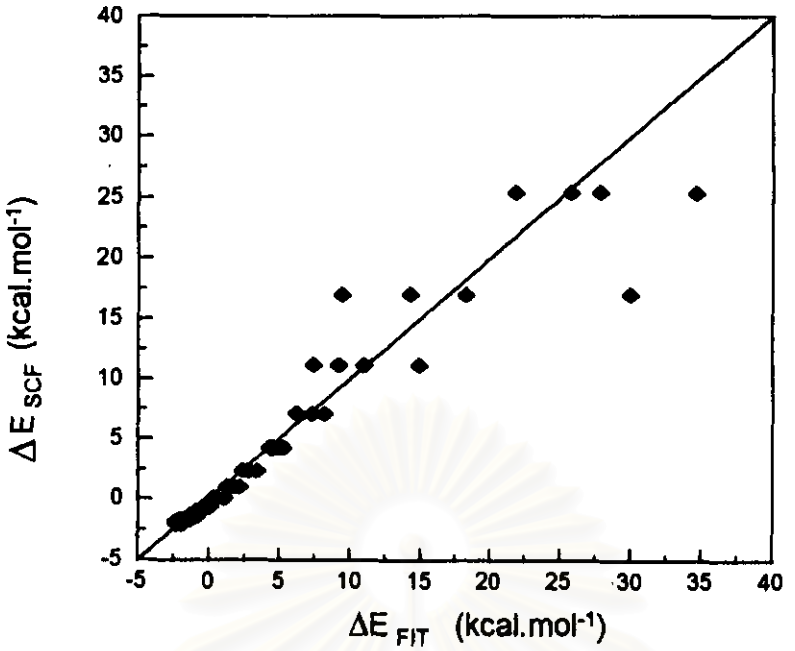

(a)

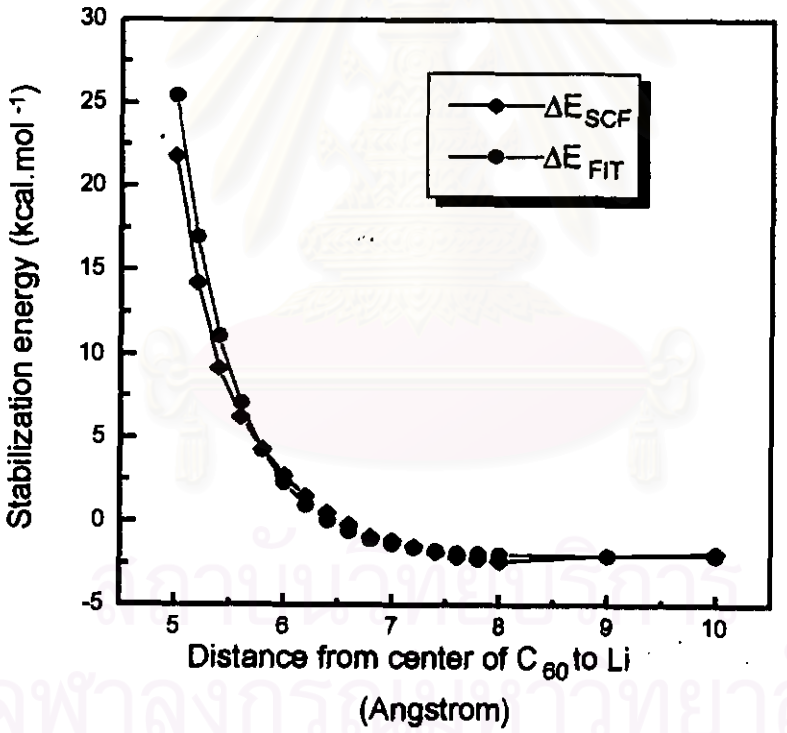

(b)

Figure 4.4 (a) Comparison of the stabilization energies for the exohedral LiC_{60} complex obtained from the SCF calculation (ΔE_{SCF}) with those from the fit (ΔE_{FIT}).

(b) ΔE_{SCF} and ΔE_{FIT} versus distance from center of C_{60} to Li for trajectory C6.

4.3 The approximation of collision energy between Li and C_{60} to form $Li@C_{60}$ complex

As describe in 3.2, the results of the fit for each trajectory for both endohedral and exohedral complexes are depicted in Fig. 4.5. The optimum functional form for the endohedral and exohedral complexes are the same as these in equation 4.1 and 4.2, respectively. The corresponding parameters are given in Table 4.4. The penetration probability calculated according to equation (2.62) as a function of $\frac{E}{V}$ are plotted in Fig. 4.6 and summarized in Table 4.4.

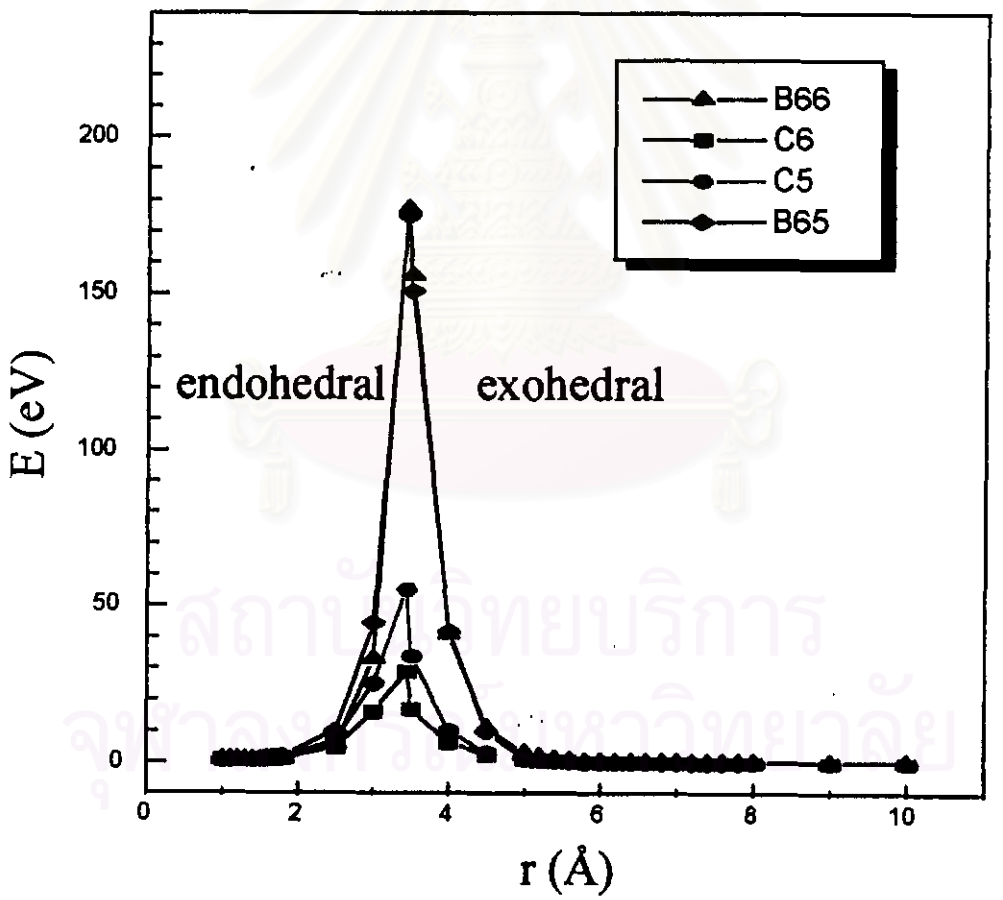

Figure 4.5 The fitted energies for the endohedral and exohedral complexes, fitted separately for each trajectory, B66, C6, C5 or B65.

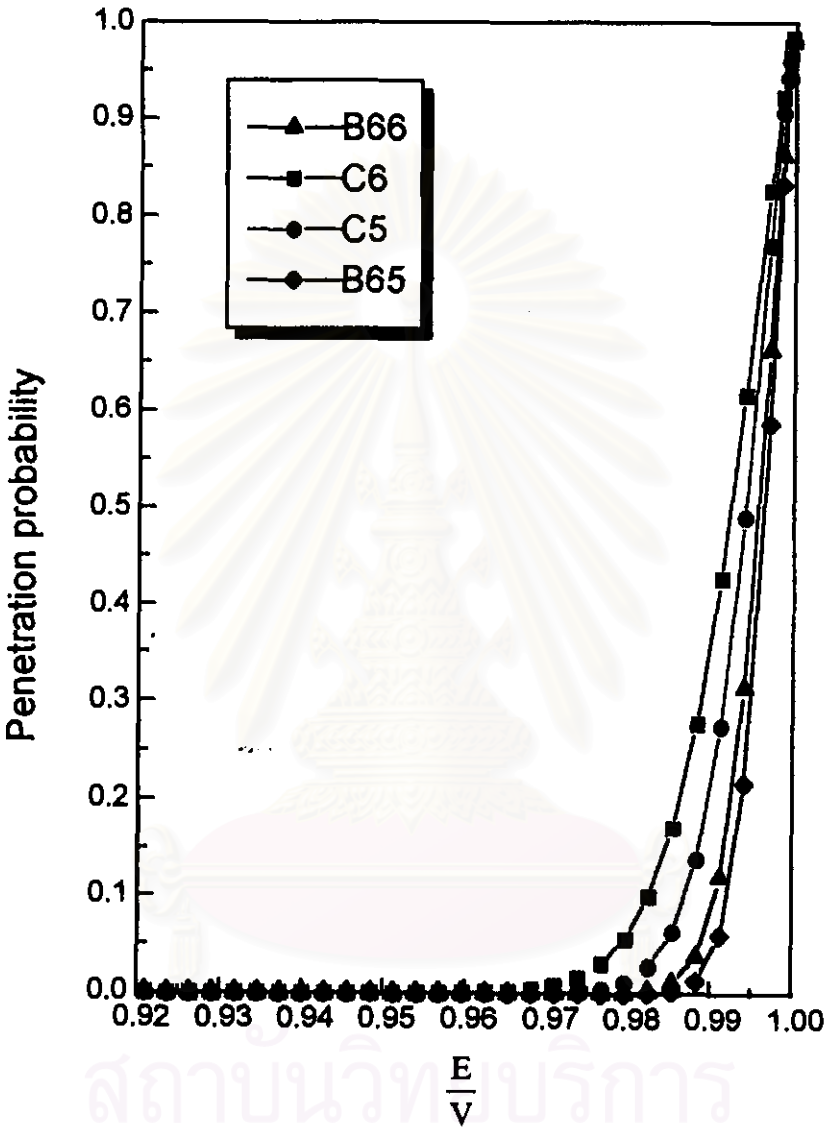

Figure 4.6 The penetration probability of collision between Li and C_{60} as a function of the ratio of collision energy (E) and the energy barrier (V).

Table 4.4 Fitted parameters *a*, *b* and *c*, standard deviation of the fits (S.D.), the distance from center of the cage to the surface (x_0) and corresponding potential ($V_{endo}(x_0)$ or $V_{exo}(x_0)$) and E/V ratio and corresponding threshold collision energy (E_t) according to equations 3.4a and 3.4b for each trajectory of endohedral and exohedral complexes, respectively.

Trajectories		*a* (eV)	*b* ($Å^{-1}$)	*c* (eV)	S.D. (eV)	x_0 (Å)	$V_{endo}(x_0)=V_{exo}(x_0)$ (eV)	E/V	E_t (eV)
B66	endo	$3.914x10^{-4}$	3.772	0.708	1.75	3.451	177.06	0.986	174.58
	exo	44.006	3.979	0.379	1.38				
C6	endo	$3.929x10^{-3}$	2.754	0.762	1.95	3.224	28.86	0.978	28.23
	exo	7.670	3.900	0.510	0.02				
C5	endo	$7.430x10^{-3}$	2.700	0.596	0.95	3.296	55.00	0.982	54.01
	exo	12.229	3.921	0.416	0.03				
B65	endo	$3.781x10^{-3}$	3.118	0.697	1.30	3.443	174.86	0.986	172.41
	exo	46.047	3.955	0.383	0.83				

4.4 Electron distribution in the Li-C_{60} complexes

When Li moves vertically from the center to the surface of C_{60} (endohedral complex), and moves furthermore outside the cage (exohedral complex) on the same direction, Li donates electron to C_{60} and electron density of each carbon atom is changed. Figure 4.7 and 4.8 display the surface and contour plots of the net charge of Li atom in endohedral and exohedral complexes, respectively. The angle shown in the plot is defined as that in Fig. 4.1. Similar plots for each carbon atoms of C_{60} are displayed in Fig. 4.9-4.12 for endohedral and Fig. 4.13-4.16 for exohedral complexes. Carbon atoms which significantly change of the net charge, compared to those of free ligand (C_{60}), are collected in Table 4.5.

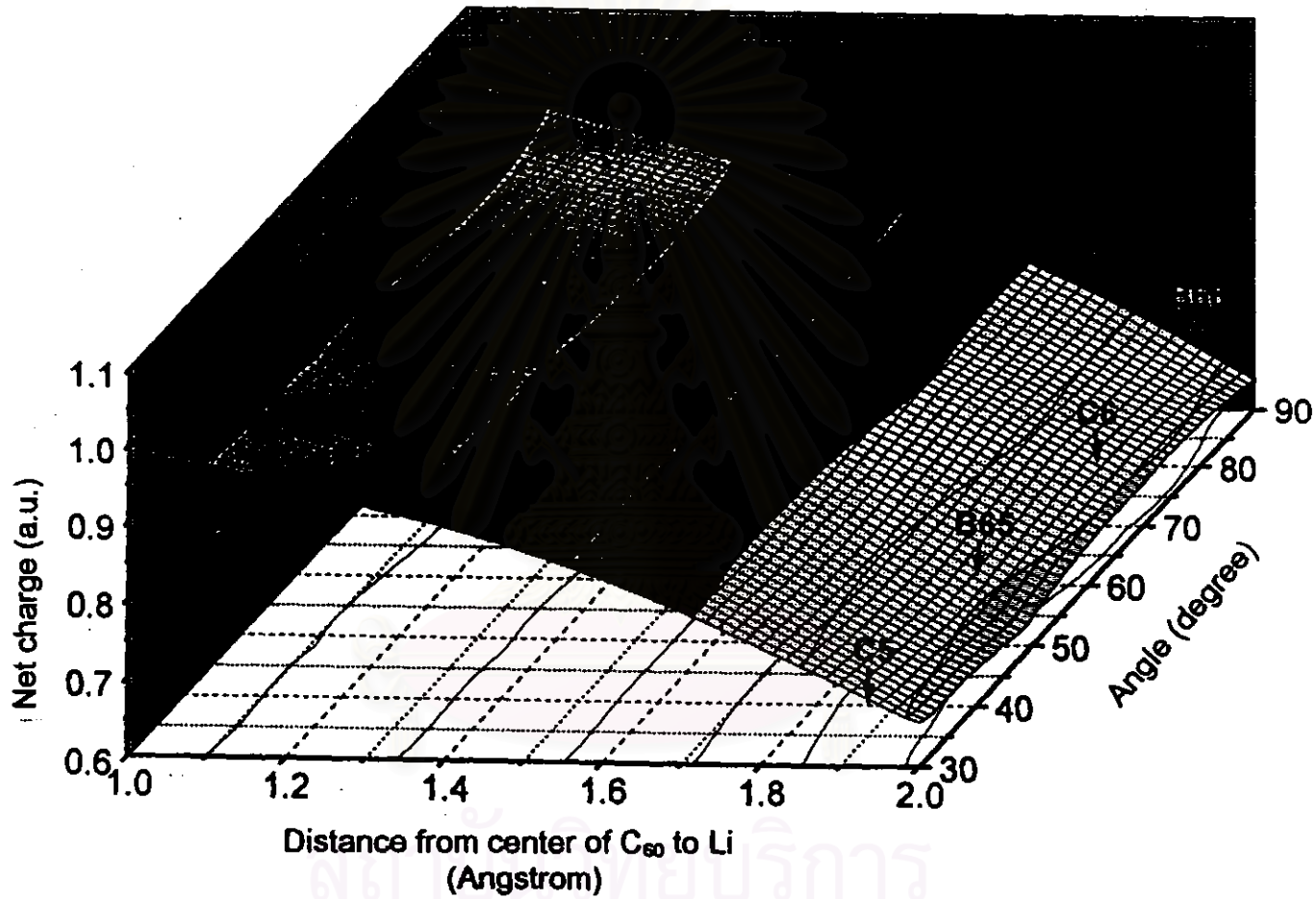

Figure 4.7 Atomic net charges for the endohedral Li@C_{60} complexes as a function of the distance from center of C_{60} to Li (see text for more detail).

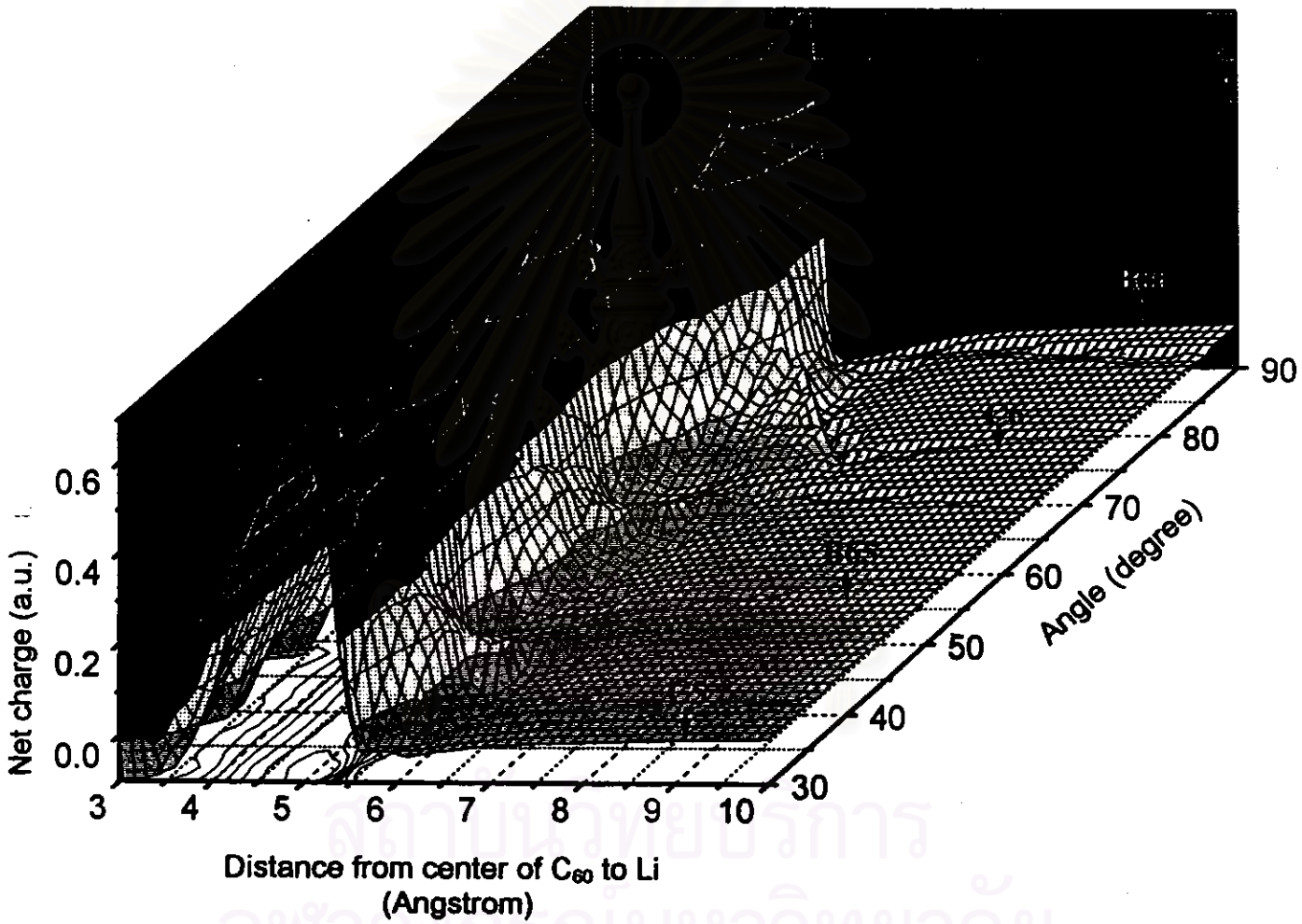

Figure 4.8 Atomic net charges for the exohedral LiC_{60} complexes as a function of the distance from center of C_{60} to Li (see text for more detail).

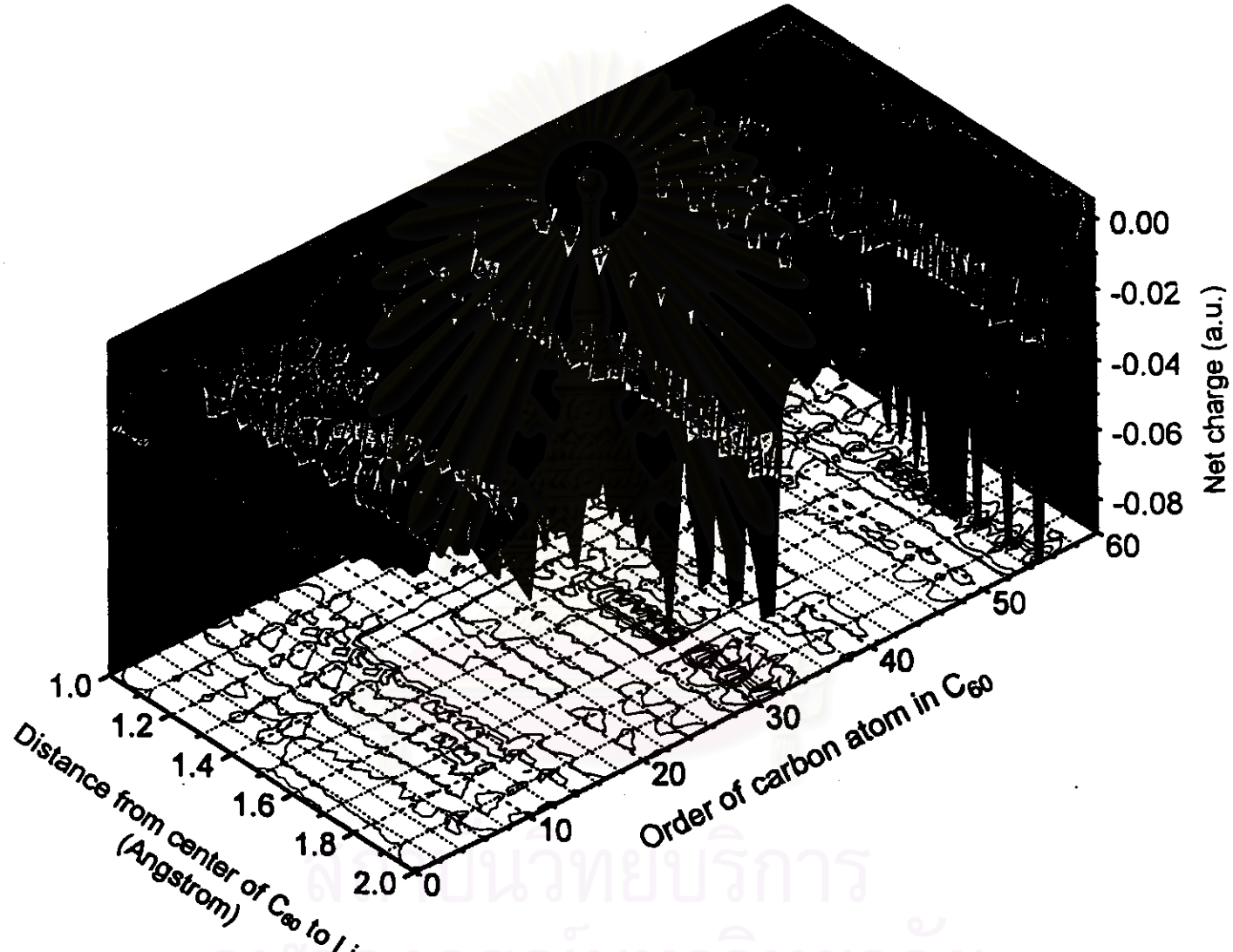

Figure 4.9 Atomic net charges of carbon atoms for the endohedral Li@C_{60} complexes in trajectory B66 as a function of the distance from center of C_{60} to Li (see text for more detail).

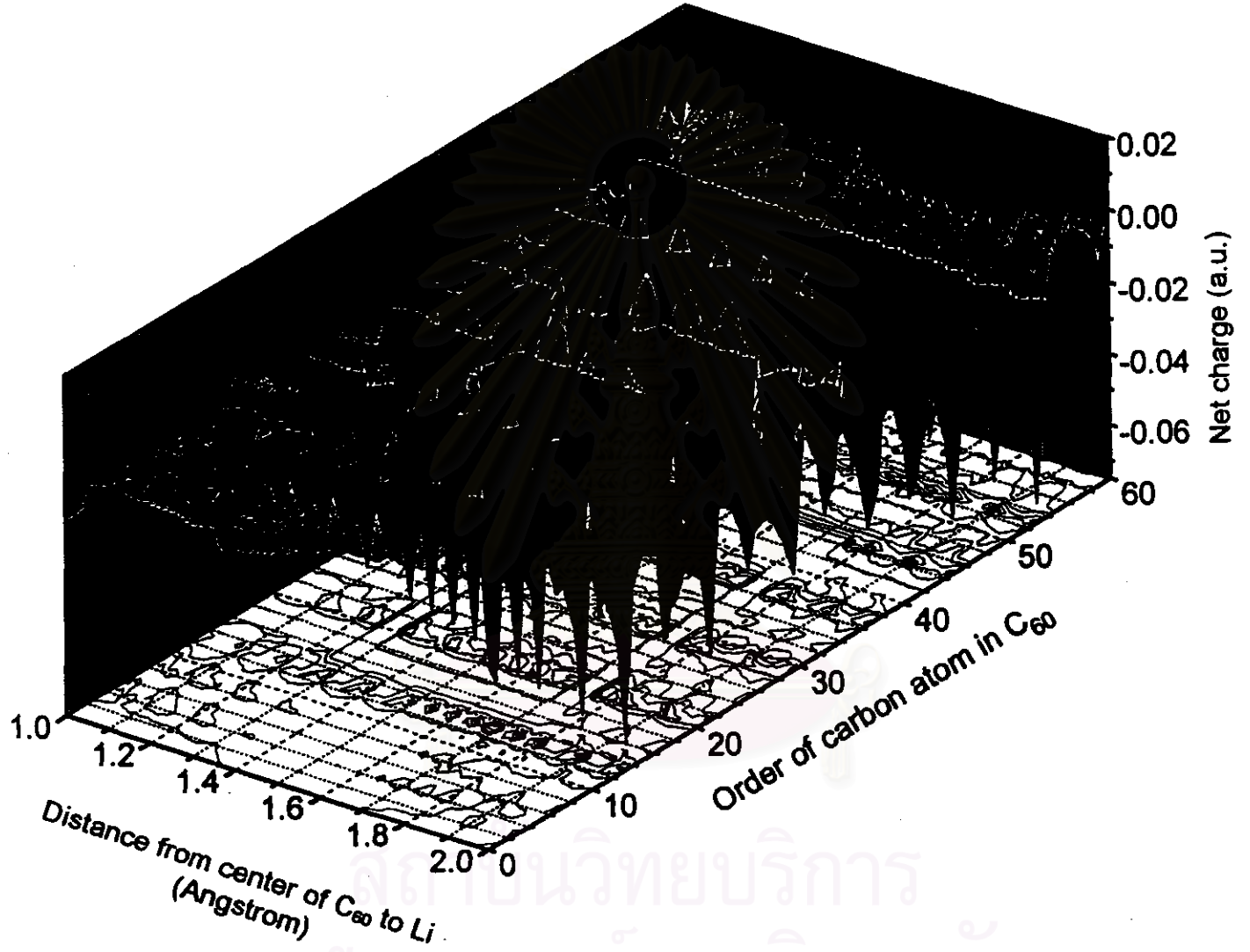

Figure 4.10 Atomic net charges of carbon atoms for the endohedral Li@C_{60} complexes in trajectory C6 as a function of the distance from center of C_{60} to Li (see text for more detail).

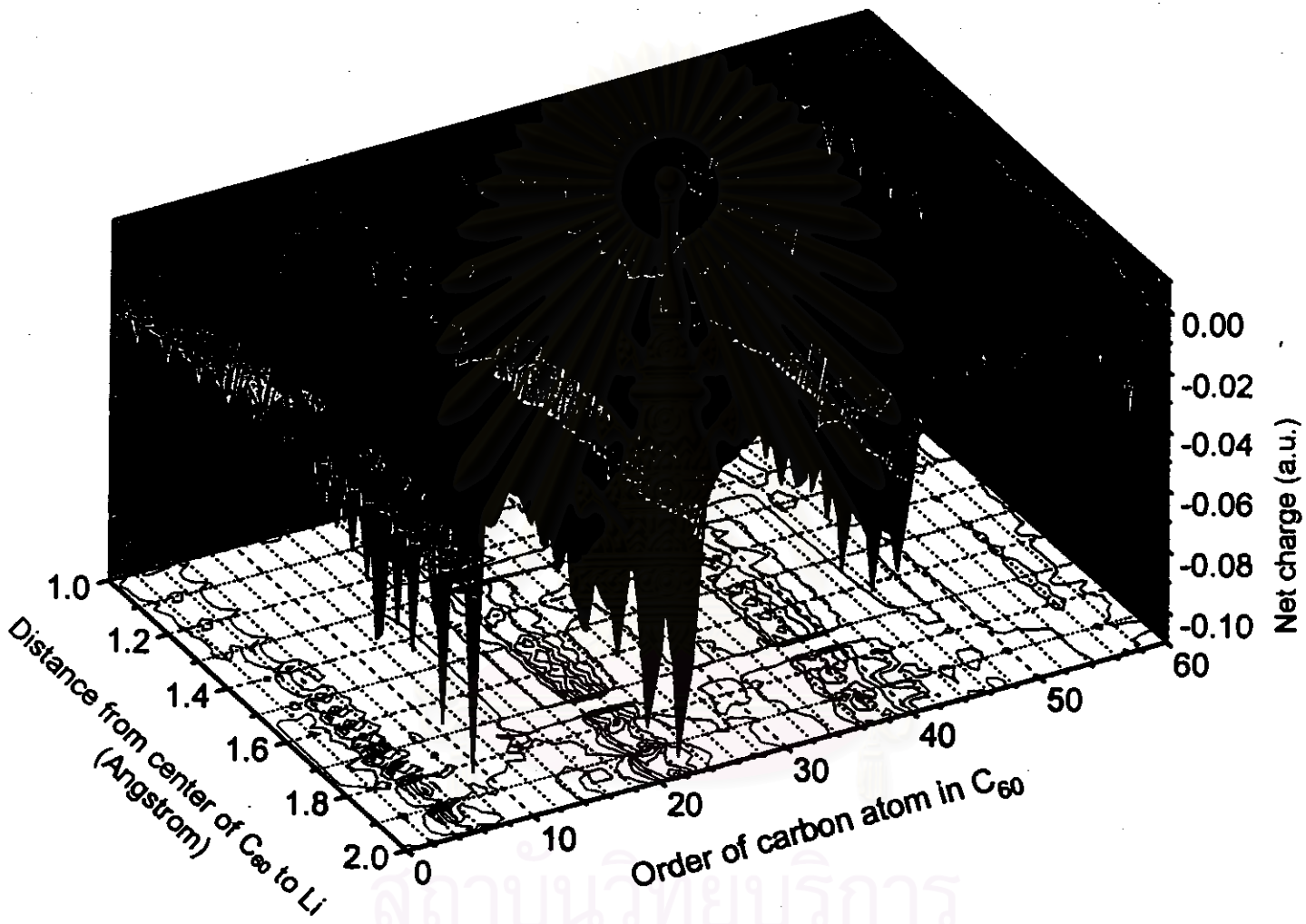

Figure 4.11 Atomic net charges of carbon atoms for the endohedral $Li@C_{60}$ complexes in trajectory C5 as a function of the distance from center of C_{60} to Li (see text for more detail).

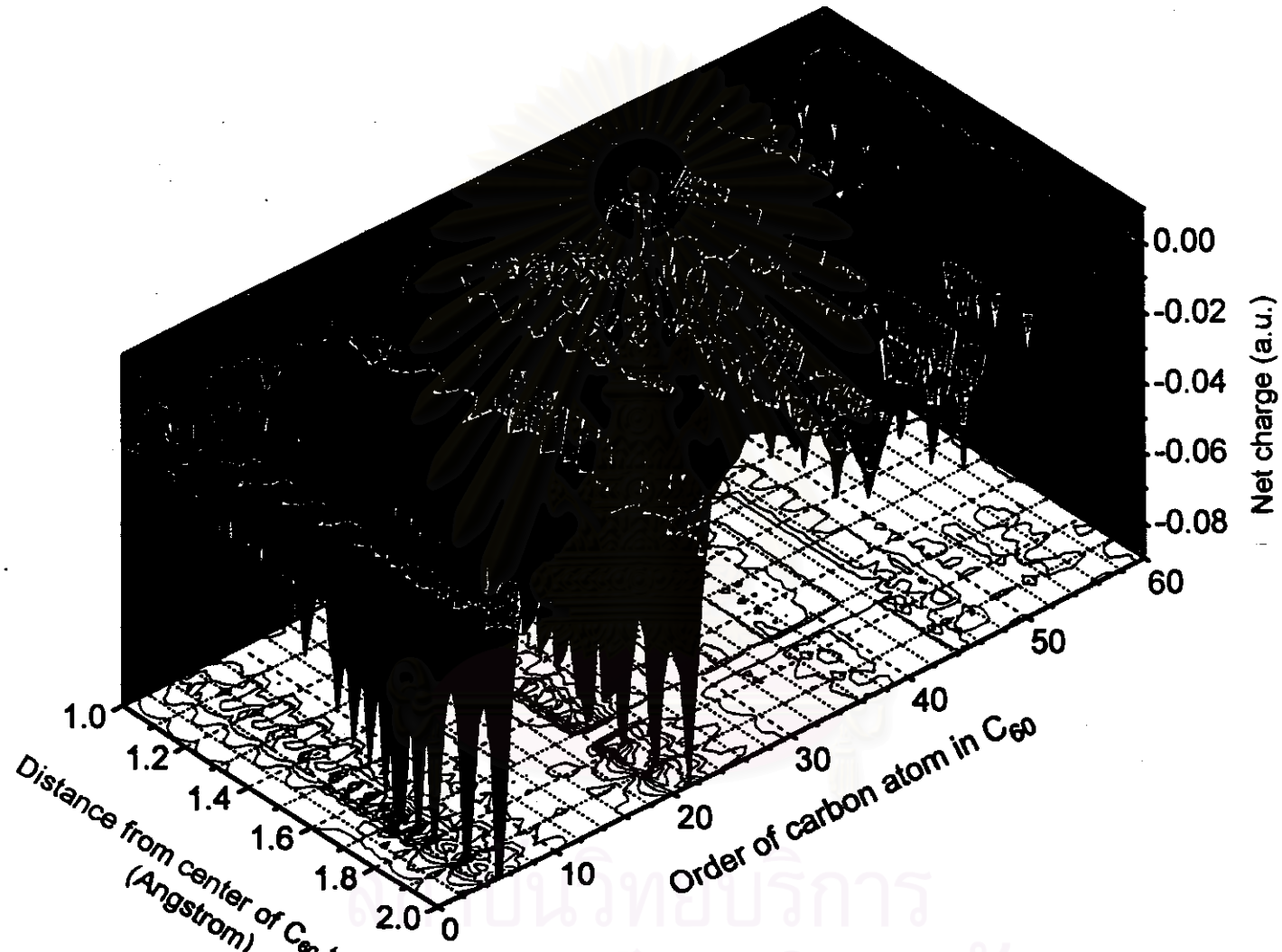

Figure 4.12 Atomic net charges of carbon atoms for the endohedral $Li@C_{60}$ complexes in trajectory B65 as a function of the distance from center of C_{60} to Li (see text for more detail).

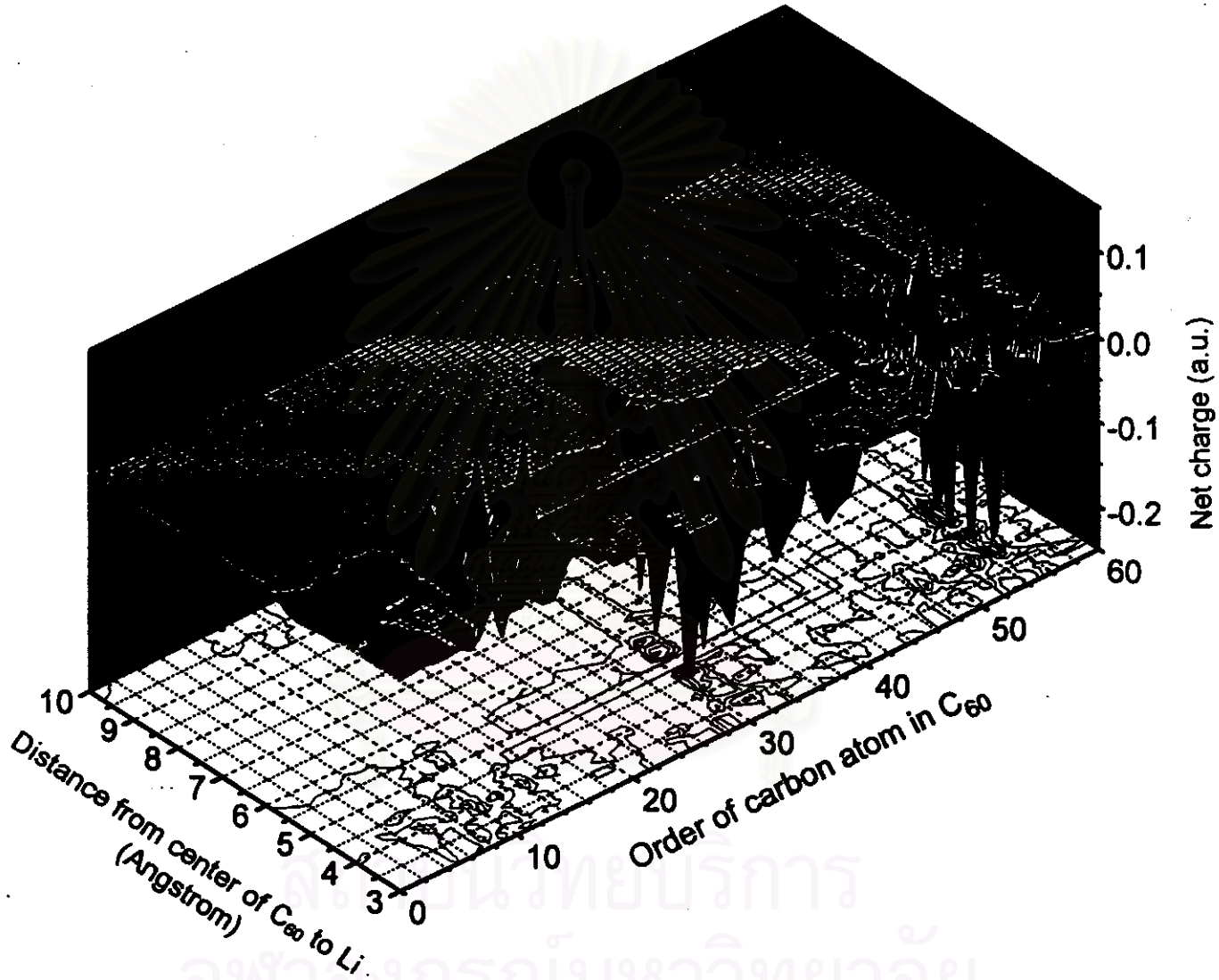

Figure 4.13 Atomic net charges of carbon atoms for the exohedral LiC_{60} complexes in trajectory B66 as a function of the distance from center of C_{60} to Li (see text for more detail).

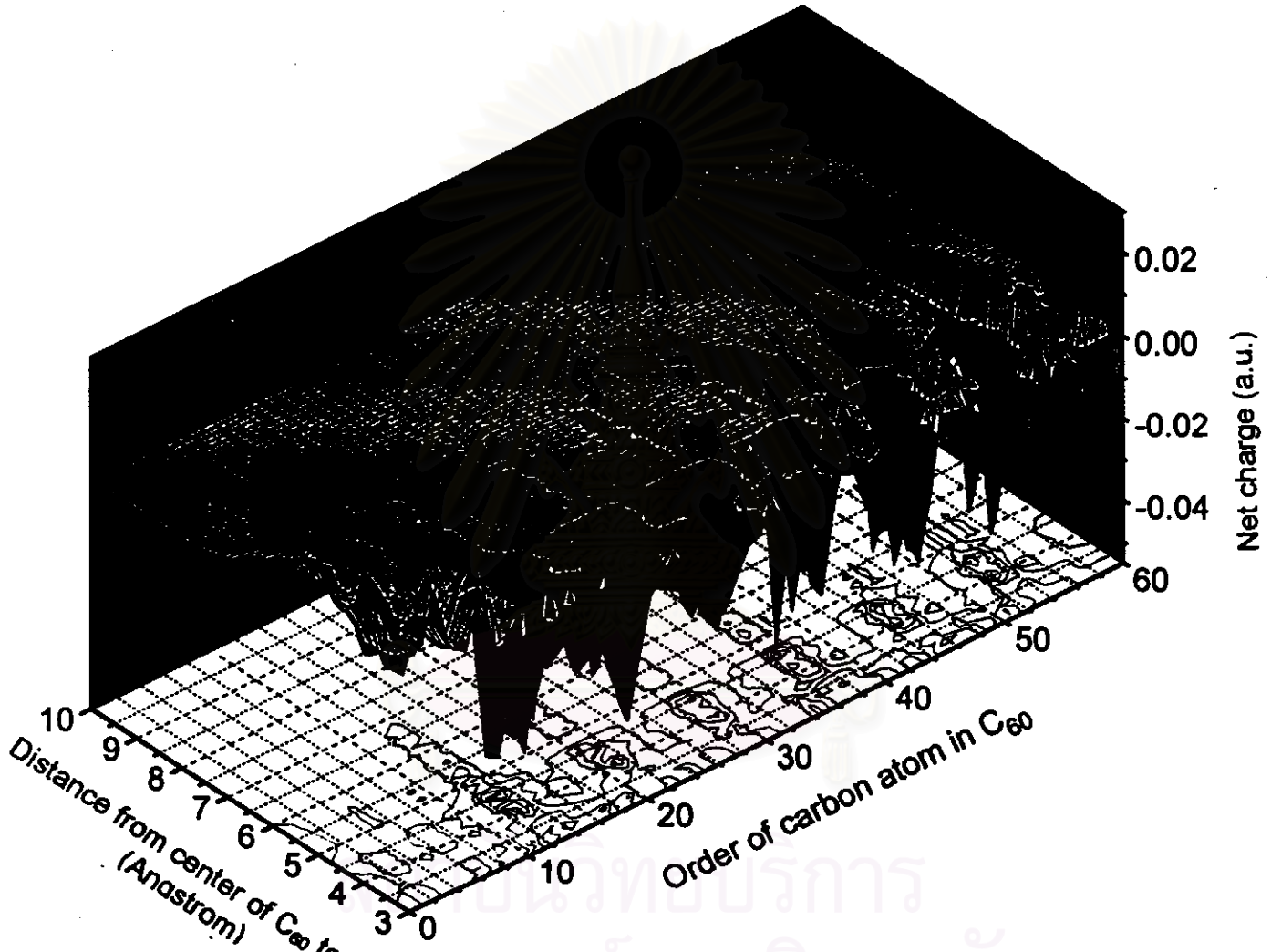

Figure 4.14 Atomic net charges of carbon atoms for the exohedral LiC_{60} complexes in trajectory C6 as a function of the distance from center of C_{60} to Li (see text for more detail).

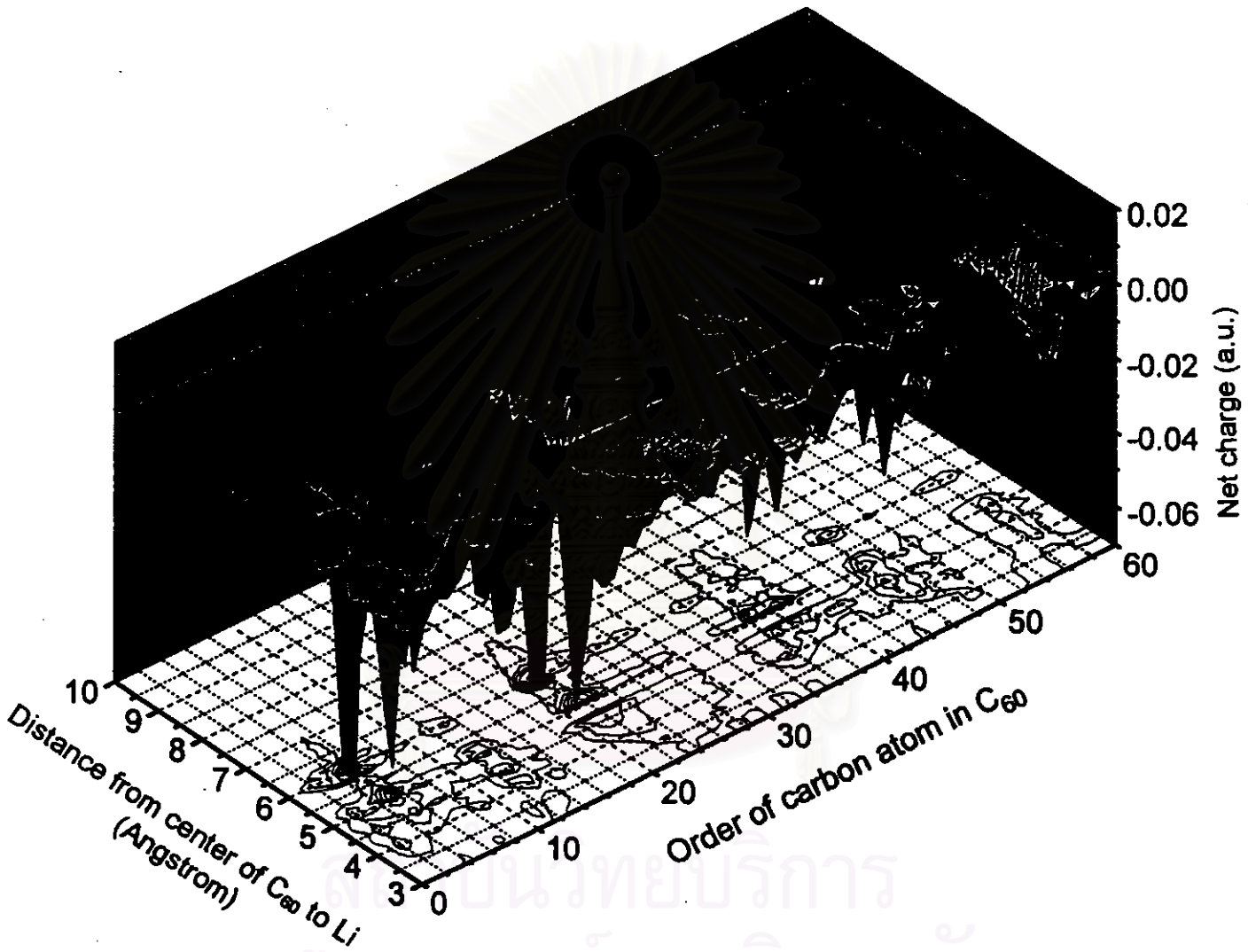

Figure 4.15 Atomic net charges of carbon atoms for the exohedral LiC_{60} complexes in trajectory C5 as a function of the distance from center of C_{60} to Li (see text for more detail).

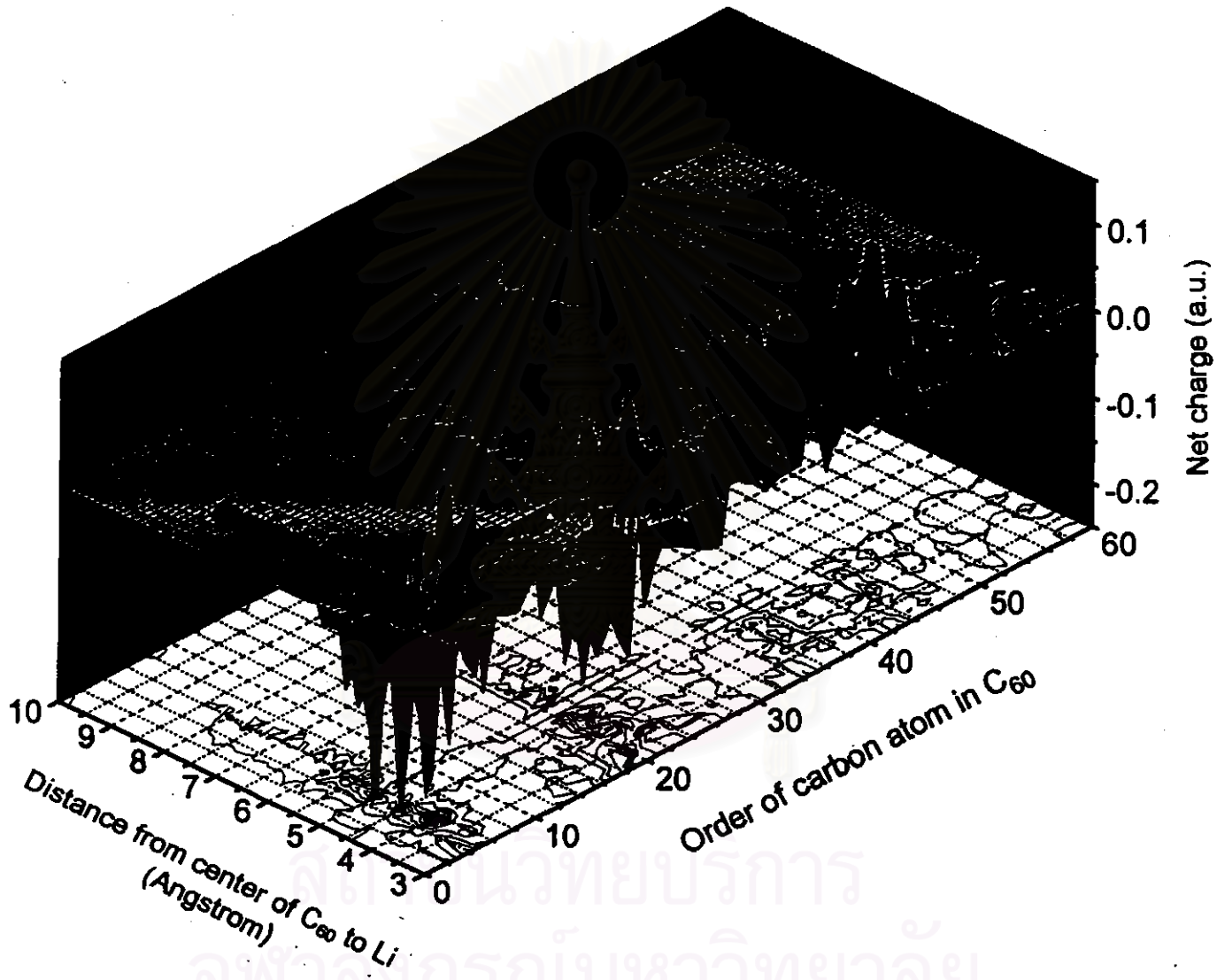

Figure 4.16 Atomic net charges of carbon atoms for the exohedral LiC_{60} complexes in trajectory B65 as a function of the distance from center of C_{60} to Li (see text for more detail).

Table 4.5 Carbon atoms (see Fig. 3.3 for atomic label) of C_{60} which display significant change of the electron density (values taken from the complexes of separation r, where $1.4 \leq r \leq 2.0$ Å for endohedral and $4.0 \leq r \leq 6.0$ Å for exohedral complexes).

Trajectory	$Li@C_{60}$	LiC_{60}
B66	9, 10, 14, 25, 29, 31, 38, 49, 53, 55	31, 55
C6	13, 21, 29, 37, 45, 53	13, 21, 29, 37, 45, 53
C5	5, 21, 22, 37, 39	5, 21, 22, 37, 39
B65	5, 6, 13, 21, 22, 37, 39, 45, 46	5, 21

4.5 Effect of dipole moment on stability of the Li-C_{60} complexes

Changes of dipole moment as a function of C_{60}-Li distances for endohedral and exohedral complexes are summarized in Table 4.6 and Table 4.7, respectively. The corresponding plots are shown in Fig. 4.17 for $Li@C_{60}$ and Fig. 4.19 for LiC_{60} complexes. To present more details of the changes, variation of the stabilization energies and the dipole moment of the $Li@C_{60}$ and LiC_{60} complexes as a function of displacements of Li in each trajectory are, again, plotted in Fig. 4.18 and 4.20, respectively.

Table 4.6 Dipole moment (μ) of the Li@C_{60} complexes for the 4 trajectories as a function of C_{60}-Li distance (r).

r (Å)	μ (Debye)			
	B66	C6	C5	B65
1.00	0.1820	1.1997	1.0056	0.3253
1.10	0.1875	1.2968	1.0244	0.3533
1.20	0.1940	1.3870	1.0416	0.3984
1.30	0.1980	1.4707	1.0621	0.4216
1.40	0.2025	1.5491	1.0984	0.4608
1.50	0.2130	1.6245	1.1215	0.4954
1.55	0.2146	1.6620	1.1406	0.5102
1.60	0.2163	1.6998	1.1525	0.5328
1.65	0.2180	1.7386	1.1648	0.5516
1.68	0.2213	1.7624	1.1812	0.5731
1.72	0.2247	1.7785	1.2002	0.6019
1.75	0.2262	1.8197	1.2185	0.6185
1.80	0.2287	1.8625	1.2352	0.6298
1.90	0.2306	1.9502	1.2520	0.6664
2.00	0.2338	2.0458	1.2712	0.7120

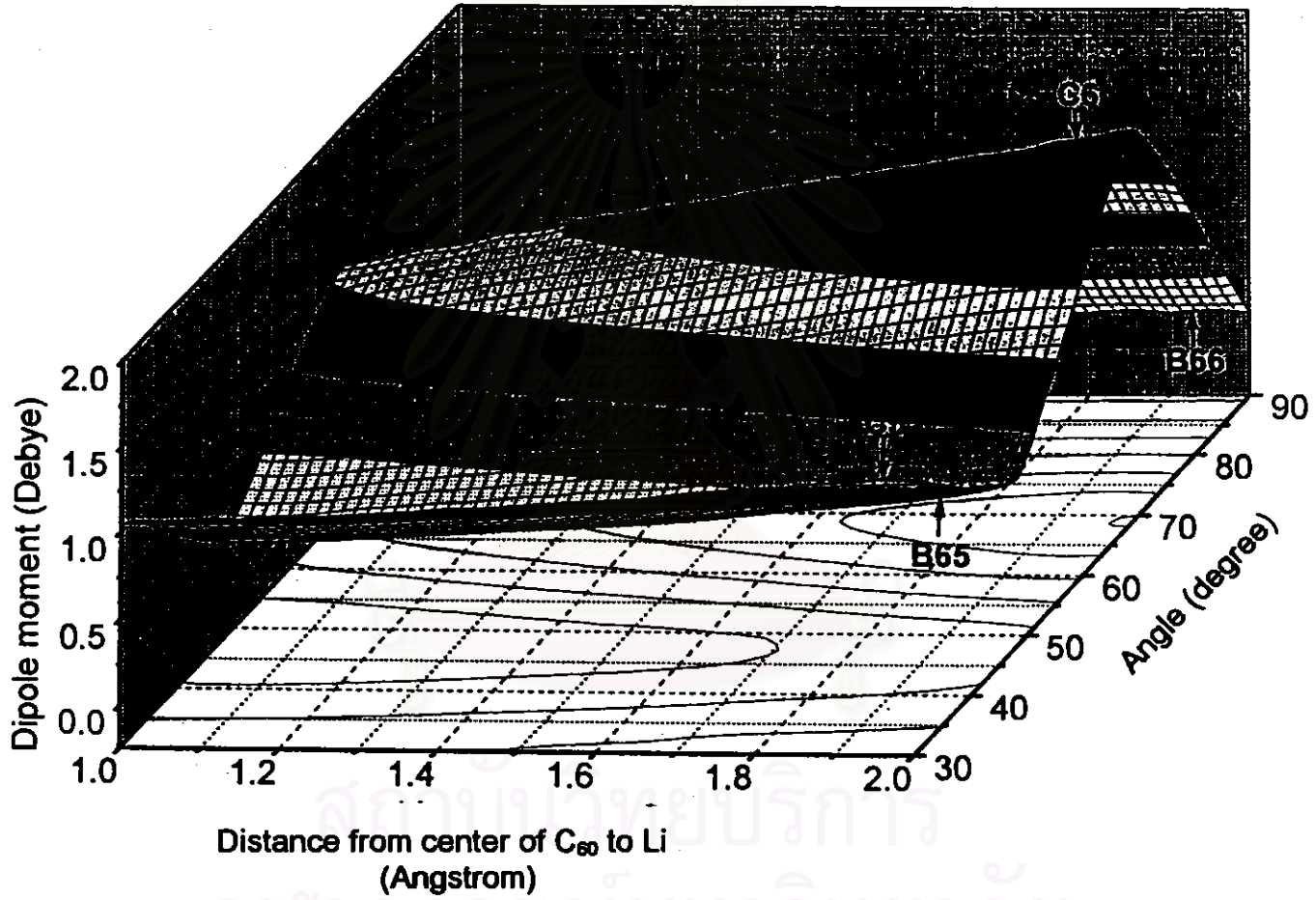

Figure 4.17 Dipole moment of endohedral Li@C_{60} complexes as a function of C_{60}-Li distances (see text for more detail).

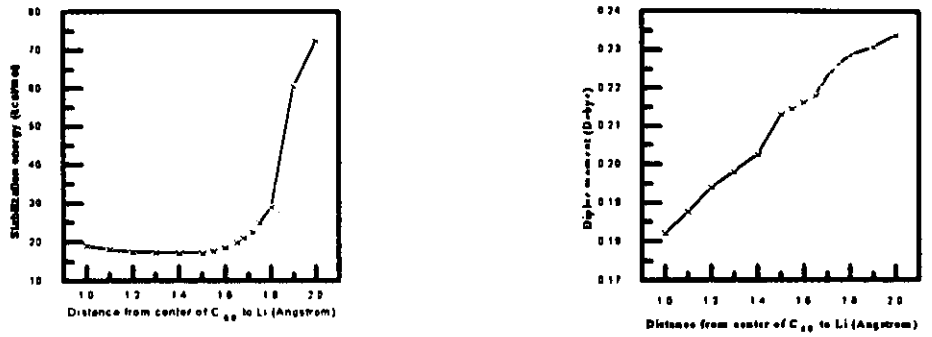

(a)

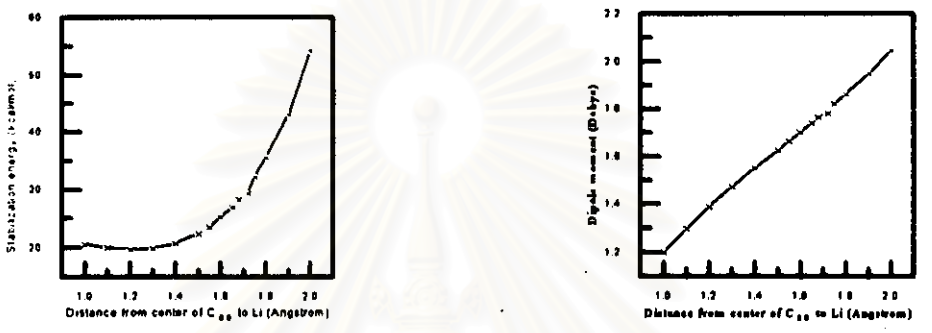

(b)

(c)

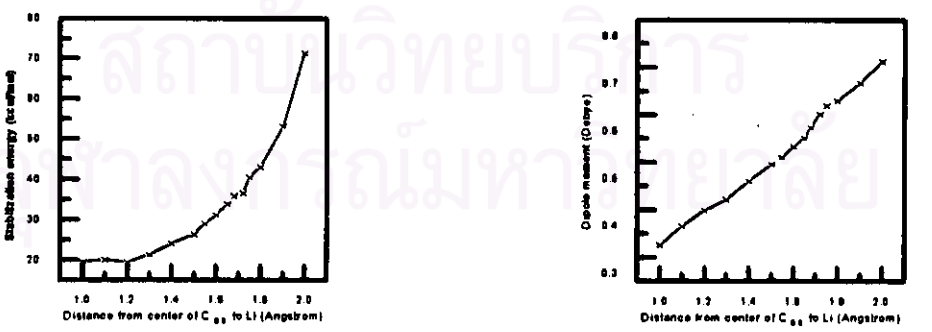

(d)

Figure 4.18 Stabilization energies and dipole moment of Li@C_{60} complexes in different paths (a) B66, (b) C6, (c) C5 and (d) B65.

Table 4.7 Dipole moment (μ) of the LiC_{60} complexes for the 4 trajectories as a function of C_{60}-Li distance (r).

r (Å)	μ (Debye)			
	B66	C6	C5	B65
3.9	0.2608	5.2535	2.1157	1.8655
4.0	0.7926	5.6149	2.5414	2.0415
4.1	1.6952	6.0649	2.9822	2.2715
4.5	4.3334	7.0576	5.0783	4.8366
5.0	7.1855	8.0891	7.8189	7.9113
5.2	8.3666	8.8046	8.7702	9.2153
5.4	9.5789	8.2963	7.8748	8.5656
5.6	10.7709	7.5806	7.3390	7.7448
5.8	7.2241	6.7405	6.5844	6.8157
6.0	6.4564	5.8372	5.7246	5.9162
6.2	5.6292	4.9320	4.8390	5.0469
6.4	4.7860	4.0762	3.9875	4.2227
6.6	3.9738	3.3097	3.1368	3.4659
6.8	3.2319	2.6483	2.5550	2.7958
7.0	2.582	2.1413	2.0473	2.2737
7.2	2.1662	1.6793	1.5879	1.9099
7.4	1.6096	1.3050	1.3198	1.4778
7.6	1.2395	1.0059	0.9244	1.0627
7.8	0.9440	0.7697	0.6941	0.8071
8.0	0.7149	0.5864	0.5180	0.6093
9.0	0.1770	0.1473	0.1118	0.1455
10.0	0.0433	0.0330	0.0189	0.0323

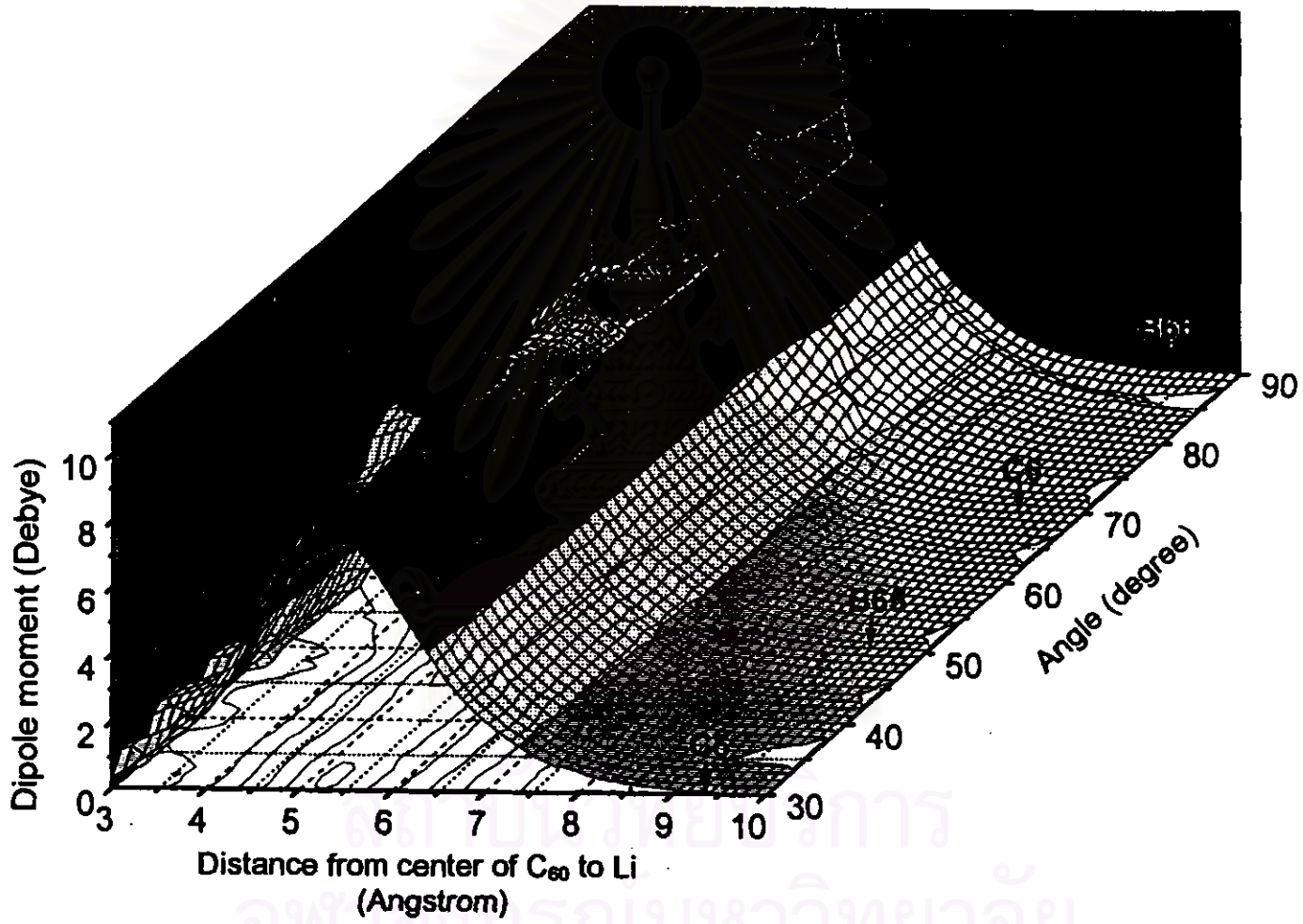

Figure 4.19 Dipole moment of exohedral LiC_{60} complexes as a function of C_{60}-Li distances (see text for more detail).

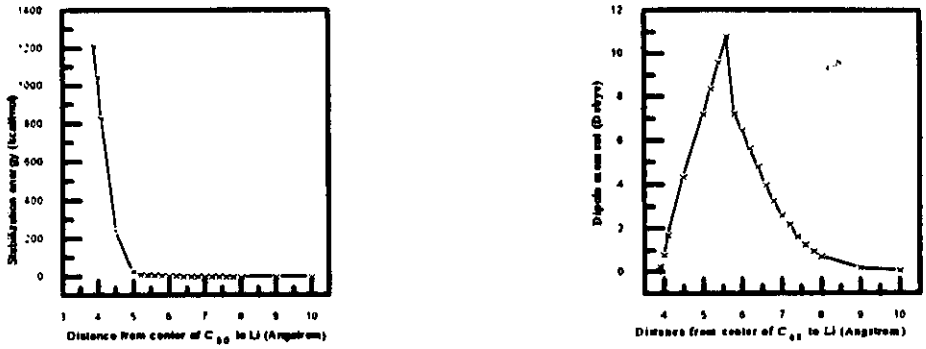

(a)

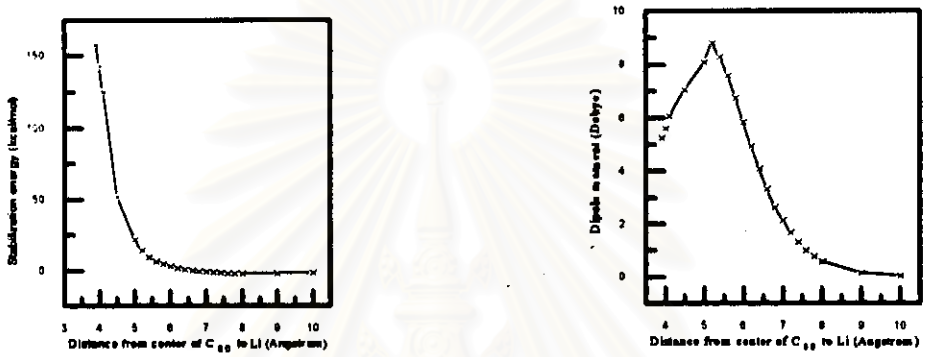

(b)

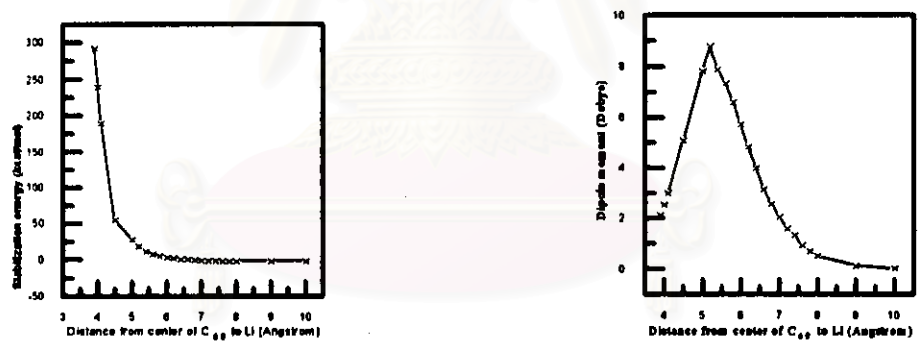

(c)

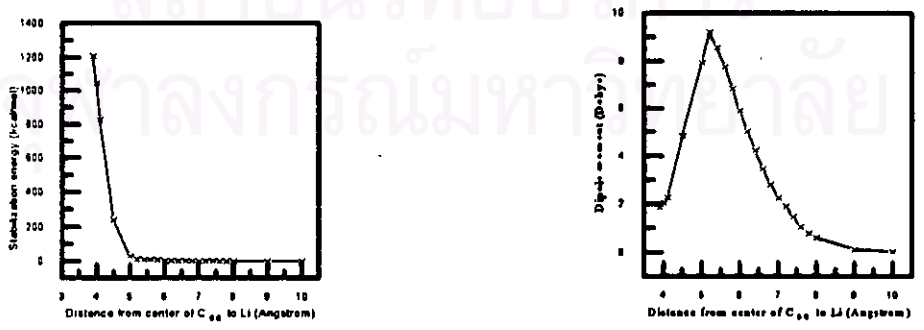

(d)

Figure 4.20 Stabilization energies and dipole moment of LiC_{60} complexes in different paths (a) B66, (b) C6, (c) C5 and (d) B65.

4.6 Optimized structures and properties of exohedral complexes

Optimized structures of the Li_nC_{60} complexes, where n=1-6 and 12 were displayed in Fig. 4.21. Characteristics of the complexes, such as stabilization energy per lithium atom ($\Delta E/n$) and HOMO-LUMO energy gap (E_g) have been analyzed and summarized in Table 4.8.

Table 4.8 Characteristics of the Li_nC_{60} complexes calculated using STO-3G (normal letter) and 6-31G (bold letter) basis sets : distance between C_{60} and Li (r); total energy (E); stabilization energy per Li atom ($\Delta E/n$) and HOMO-LUMO energy gap (E_g).

Molecule	Symmetry	Valence orbitals	Spin state	Characteristics					
				r (Å)	C=C (Å)	C-C (Å)	E (Hartrees)	ΔE/n (eV)	E_g (eV)
C_{60}	I_h	closed shell	singlet	-	1.375	1.458	-2244.2212	-	8.6518
				-	**1.370**	**1.448**	**-2270.9711**	-	**7.5562**
LiC_{60}	C_{3v}	a_1^1	doublet	5.24	1.376	1.463	-2251.5674	-0.8350	6.2417
				7.38	**1.375**	**1.452**	**-2278.4080**	**-0.4923**	**4.8512**
Li_2C_{60}	D_{3d}	e_u^2	triplet	5.47	1.377	1.462	-2258.9309	-1.0884	5.8412
				7.51	**1.376**	**1.452**	**-2285.8802**	**-0.8012**	**4.3624**
Li_3C_{60}	C_{3v}	$a_2^1e^2$	quartet	5.51	1.376	1.462	-2266.3199	-1.3914	5.3341
				7.55	**1.375**	**1.452**	**-2293.3654**	**-1.0254**	**4.1212**
Li_4C_{60}	C_{3v}	$a_2^2e^2$	triplet	5.60	1.379	1.461	-2273.7447	-1.7868	5.7278
				7.62	**1.374**	**1.452**	**-2300.8771**	**-1.3168**	**4.3007**
Li_5C_{60}	C_{3v}	$a_2^2a_2^1e^2$	quartet	5.73	1.378	1.463	-2281.1774	-2.0672	6.0778
				7.88	**1.375**	**1.452**	**-2308.1707**	**-1.5235**	**4.6518**
Li_6C_{60}	C_{3v}	$a_2^1a_2^1e^2e^2$	heptet	5.82	1.378	1.462	-2288.6535	-2.4450	6.3047
				7.95	**1.374**	**1.451**	**-2315.9434**	**-1.8019**	**4.7666**
$Li_{12}C_{60}$	I_h	closed shell	singlet	5.66	1.379	1.463	-2333.9345	-4.3714	5.4427
				7.64	**1.373**	**1.452**	**-2361.5544**	**-3.2216**	**4.2992**

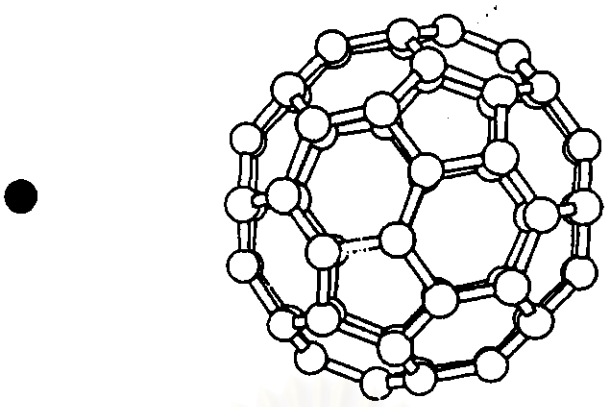

(a) LiC_{60}

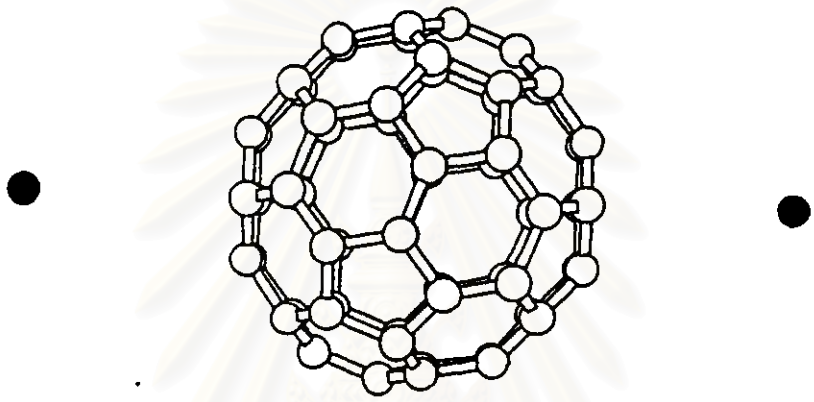

(b) Li_2C_{60}

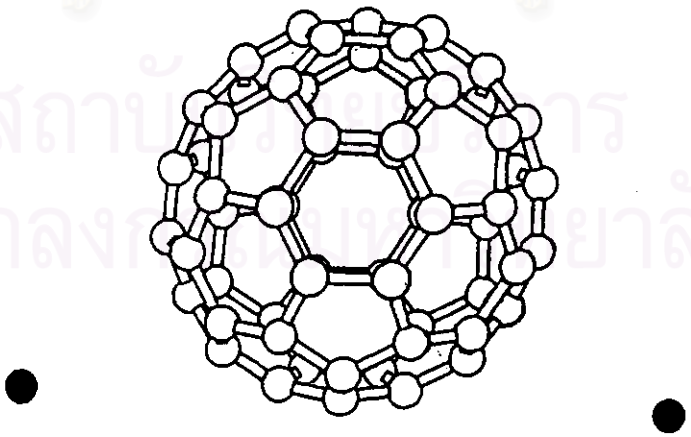

(c) Li_3C_{60}

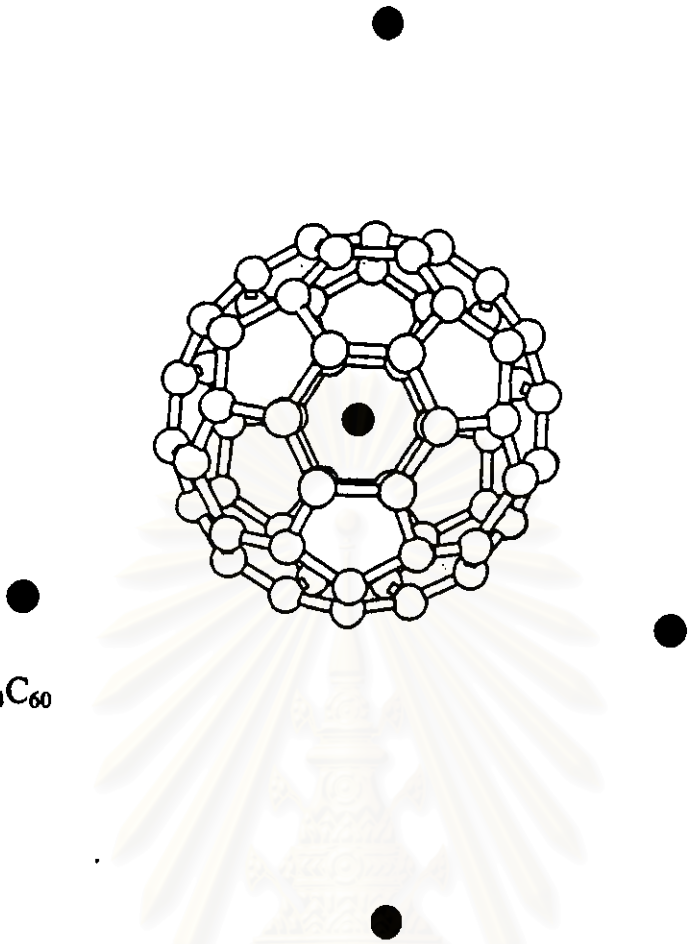

(d) Li_4C_{60}

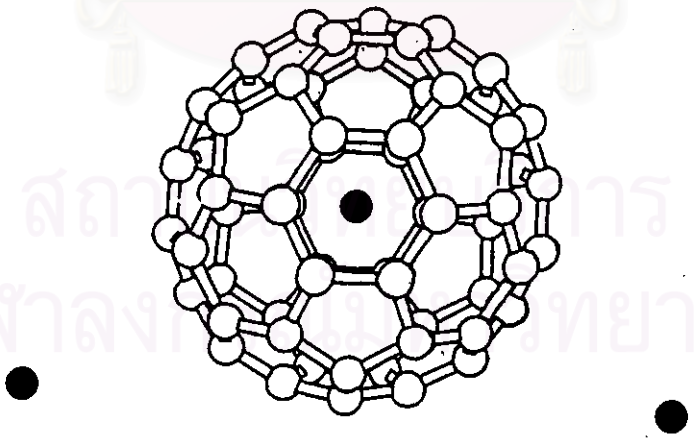

(e) Li_5C_{60}

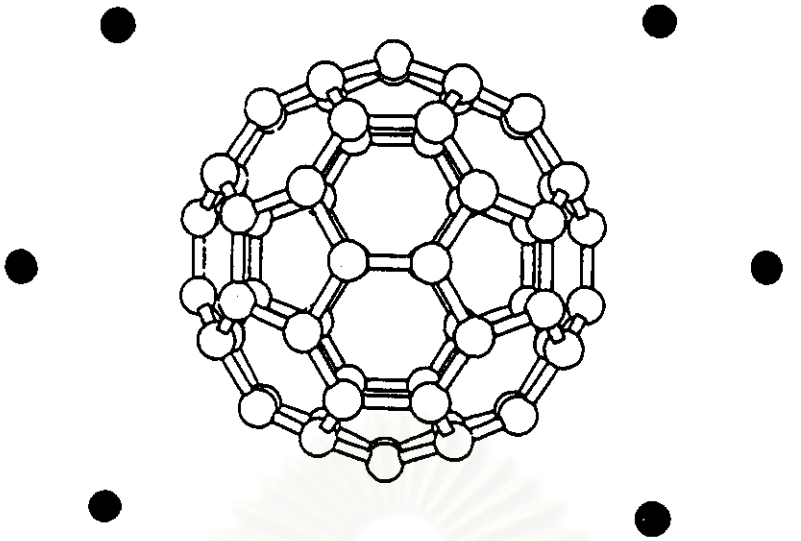

(f) Li_6C_{60}

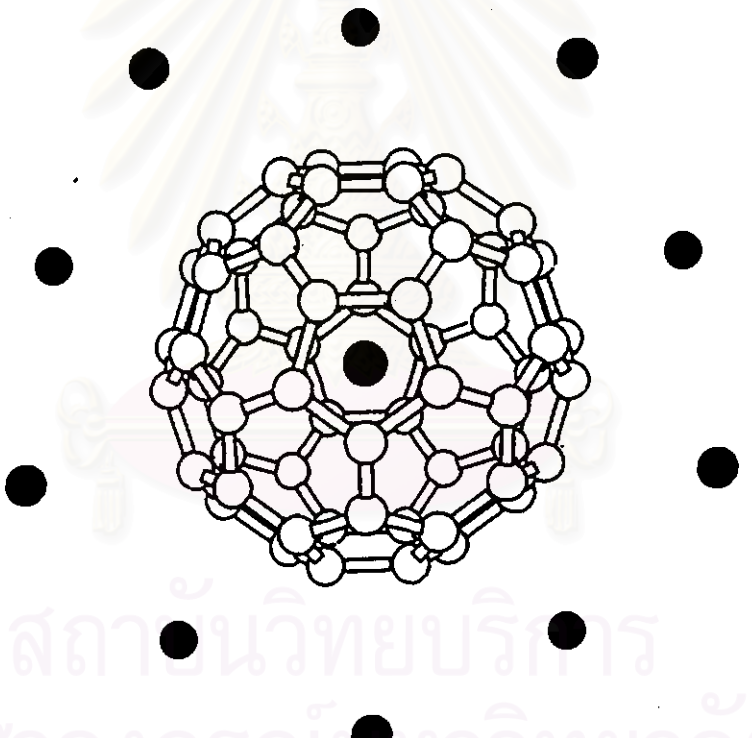

(g) $Li_{12}C_{60}$

Figure 4.21 Li_nC_{60} configurations, where (a)-(g) for n=1-6 and 12, respectively.

4.7 Electronic structures of exohedral complexes

It is known that C_{60} is a good electron acceptor. SCF calculations on the Li_nC_{60}, n=1-6 and 12, allow us to investigate electron transfer between the two species as well as changes of molecular geometry of C_{60}. Results of the calculations using both STO-3G and 6-31G basis sets have been analyzed and displayed in terms of energy level diagram (Fig. 4.22). Change of HOMO-LUMO energy gaps as a function of number of lithium atom has been plotted in Fig. 4.23.

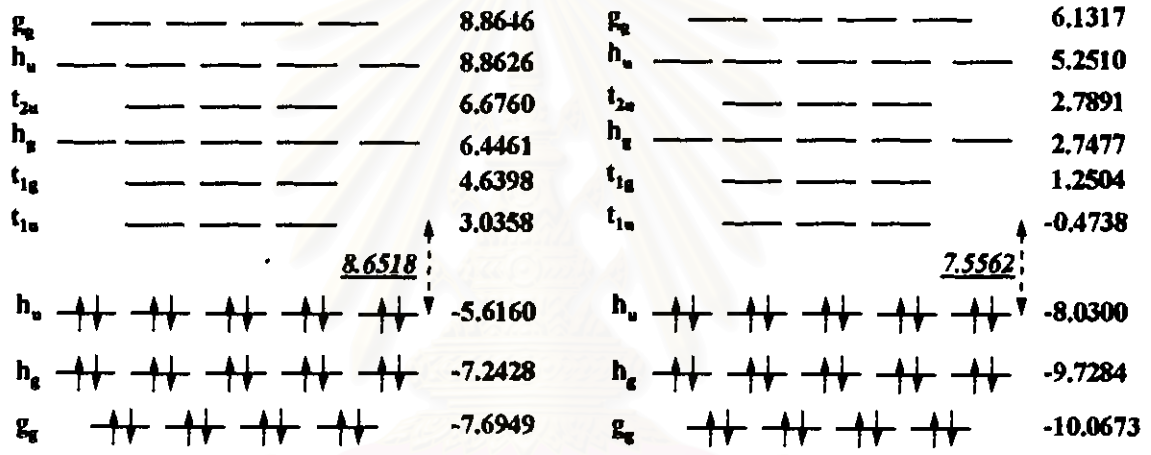

(a) C_{60}

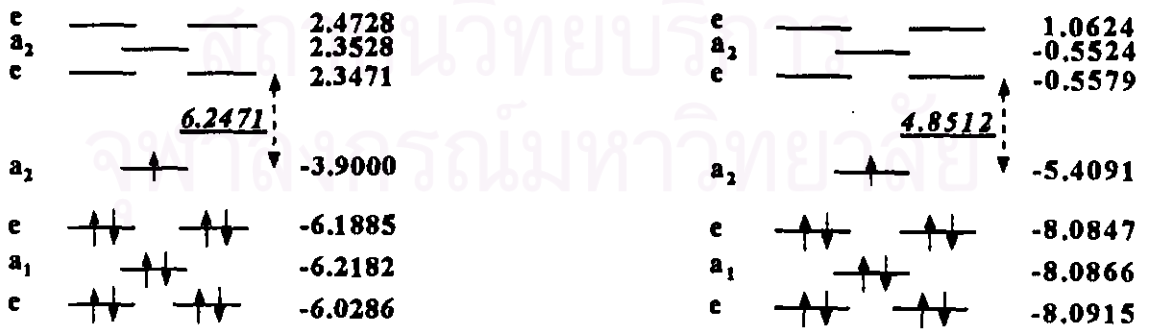

(b) LiC_{60}

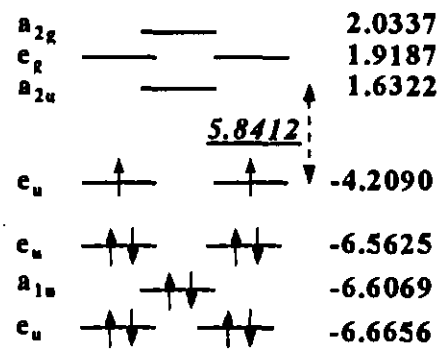

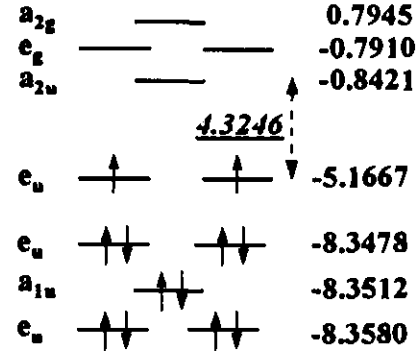

(c) Li_2C_{60}

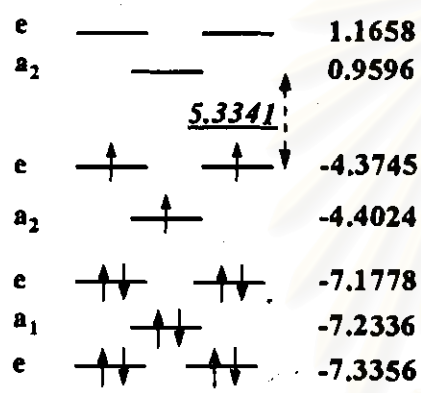

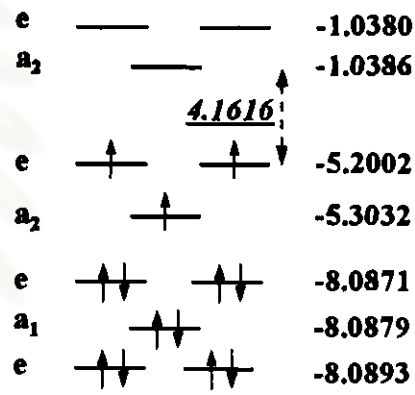

(d) Li_3C_{60}

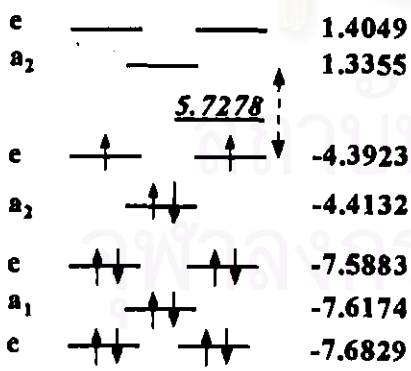

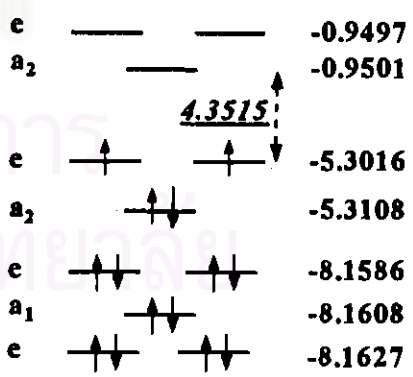

(e) Li_4C_{60}

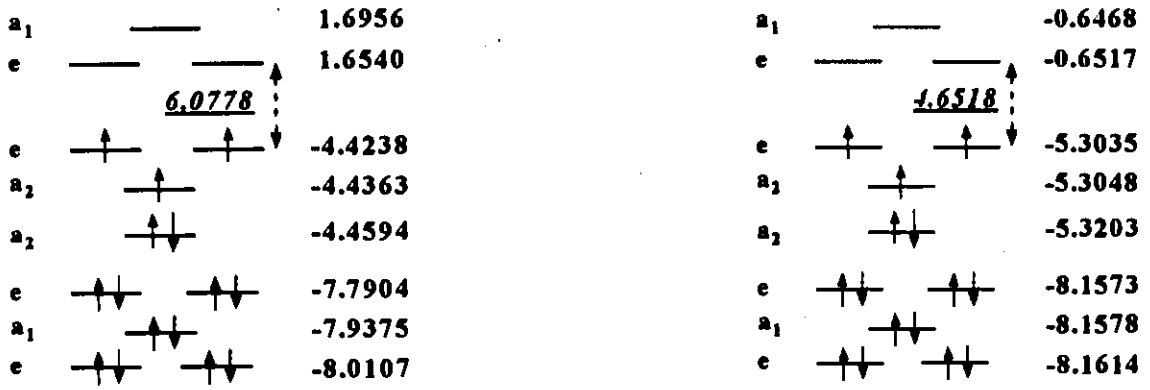

(f) Li_5C_{60}

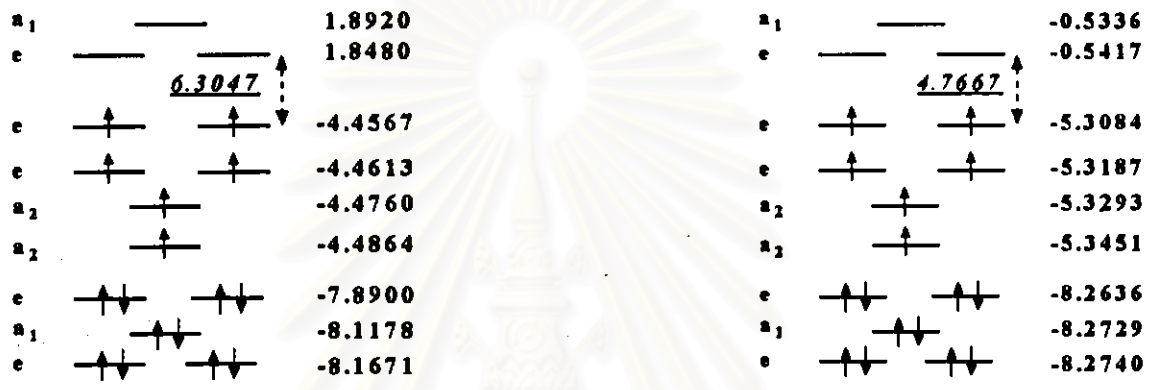

(g) Li_6C_{60}

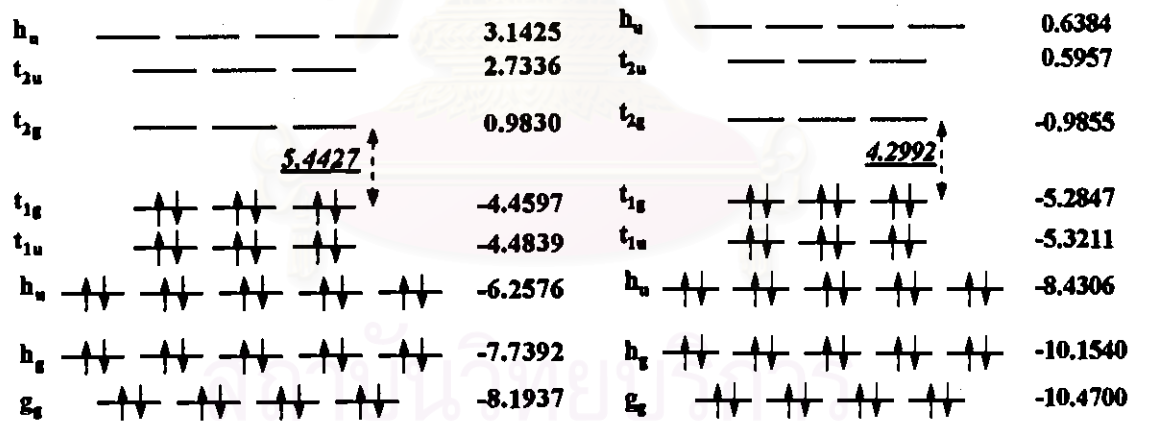

(h) $Li_{12}C_{60}$

Figure 4.22 Diagram of molecular orbital levels near the frontier of C_{60} and Li_nC_{60} complexes; calculated using STO-3G (left) and 6-31G (right) basis sets.

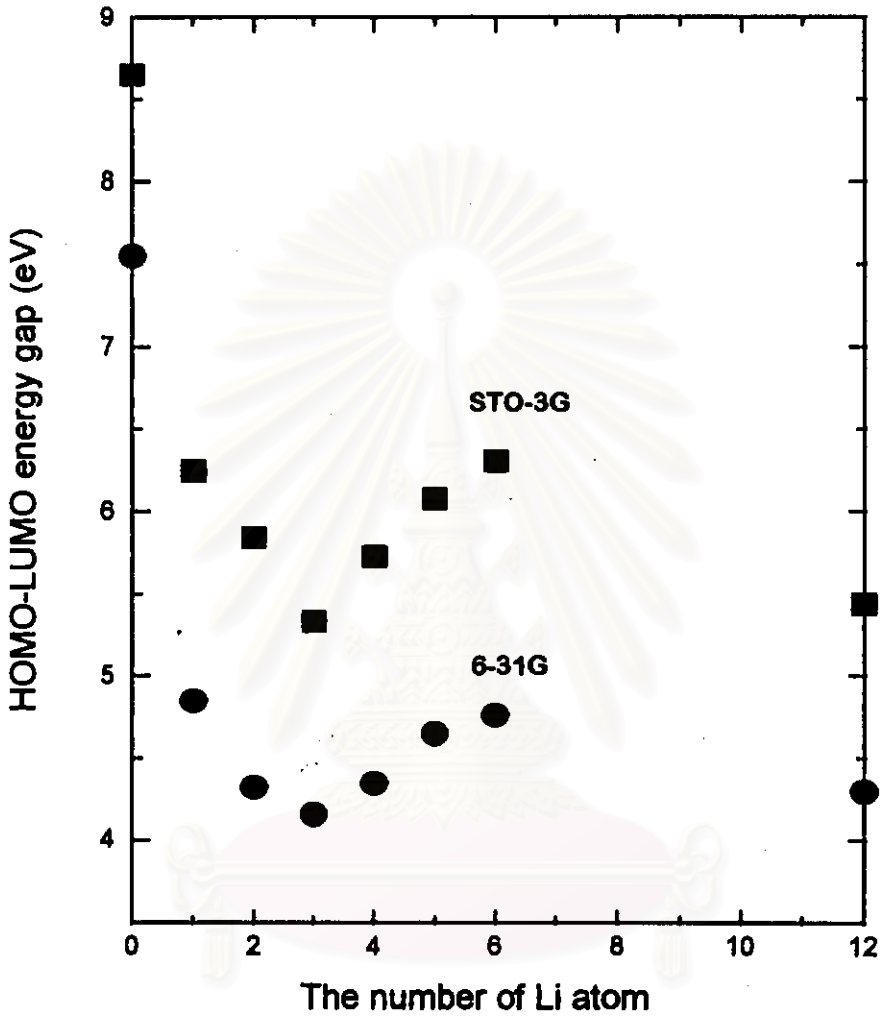

Figure 4.23 HOMO-LUMO energy gap of C_{60} and Li_nC_{60}, plotted versus the number of Li.